ELSEVIER

Thermochimica Acta 327 (1999) 63–102

thermochimica acta

Review

A review of synthetic, thermoanalytical, IR, Raman and X-ray studies on metal selenites

V.P. Verma[1]

Applied Chemistry Department, Regional Engineering College, Srinagar, Kashmir, India

Received 15 October 1998; accepted 15 October 1998

1. Introduction

Although much has been reported [1] about the metal sulphites, relatively little has appeared about the selenites. The absence of a review on selenites and the emerging importance of Se in various forms prompted the present work.

Among the early researchers in this field, Ray and Gosh [2] attributed the inability of the SeO_3^{2-} ligand to form stable complexes to the increased mass of the ion and decreased electronegativity of selenium with respect to sulphur and sulphite. Riley [3] prepared $Co(NH_3)_5SeO_3Cl$, but stated that the selenite group was readily displaced by water. Derbisher [4] reported a platinum(IV)–selenite complex, and Toropova [5] showed the existence, in solution, of selenite complexes of mercury, cadmium and silver.

In investigations of a more general nature, Geering et al. [6] have shown that the solubility of selenium in soils indicates that the selenium concentration in solution is governed by an iron(III) oxide–selenite absorption complex.

In 1964, Sathianandan et al. [7] brought together spectral information on the then available selenites and selenates and interpreted the features characteristic of the SeO_4^{2-} and SeO_3^{2-} ions. They also identified features of the spectra related to the presence of water in the solids and their thermal decomposition effects. Very recently Harrison et al. [8–10] have reported the syntheses and structures of several new, layered selenite materials based on the hexagonal tungsten-oxide motif of corner-sharing octahedra.

The synthesis and characterization of metal selenites is reported in Section 2. Selenite compounds of each of the principal characteristic groups of the Periodic Table are discussed in separate sub-sections. Selenites of all the alkali metals and alkaline earth metals have been reported and selenites of most of the p-block metals are known. Many selenite compounds of transition series and inner transition series metals have been studied, but selenites of many of the second and third row transition metals and of the lanthanide and actinide elements do not appear to have been the subject of syntheses and investigations.

In Section 3, thermal studies of selenite compounds of metals are discussed. Section 4 reports published structural studies of selenites involving X-ray diffractometry and infrared and Raman spectroscopy. Miscellaneous studies on hydrogen selenites are the subject of Section 5 and recent developments and possible avenues for further investigation are discussed.

2. Syntheses

The selenite anion has been shown to be a versatile ligand. Depending on the synthesis conditions, crystalline solids containing selenite, SeO_3^{2-}, hydrogen selenite, SeO_3H^-, and diselenite, $Se_2O_5^{2-}$, anions can be prepared [11].

[1]Present address. Camp Classes, Canal Road, Jammu, Pin 180001, India. Tel.: +91-191-547469; fax: +91-191-546297.

0040-6031/99/$ – see front matter
PII: S0040-6031(98)00577-2

2.1. Synthesis of alkali metal selenites

The heterogeneous M_2SeO_3–H_2SeO_3–H_2O (M = Li, Na, K, Rb or Cs) systems have been studied [12]. From the ΔG° values, the stability of hydrogen selenites and trihydrogen bis(selenites) increases from lithium to cesium and also, except for cesium salts, on transition from $MHSeO_3$ to $MH_3(SeO_3)_2$. The $NaHSeO_3{\cdot}3H_2O$ adduct has also been prepared and studied [13].

As part of a systematic study of compounds with potential ferroelectric properties, Micka et al. [14] studied the solubility of the K_2SeO_3–H_2SeO_3–H_2O system. They also refined the conditions for the formation of $KHSeO_3$, $KH_3(SeO_3)_2$, $K_5H_3(SeO_3)_4$ and $K_2Se_2O_5$. Muspratt [15] described $(NH_4)_2SeO_3$, $(NH_4)_2SeO_3{\cdot}H_2O$ and $(NH_4)H_3(SeO_3)_2$.

Eysseltova et al. [16] developed a computerised method for the solubility study of ternary systems. Computer programs were written to construct the solubility isotherm and to identify equilibrium. The method was tested on the K_2SO_4–$MgSO_4$–H_2O system and applied to the study of solubility isotherm at 298 K in the glycine–H_2SeO_3–H_2O system. A glycine–H_2SeO_3 compound was prepared.

Jokuziene [17] prepared ammonium selenite electrolytically.

2.2. Synthesis of alkaline earth metal selenites

Syntheses and properties of alkaline earth selenites have been described by many authors [18–26]. Losoi and Valkonen [26] synthesized $MgSeO_3{\cdot}6H_2O$, $CaSeO_3{\cdot}H_2O$, $BaSeO_3$, $BaSe_2O_5$ and $Ba(HSeO_3)_2$ using the technique of gel growth. $Mg(HSeO_3)_2{\cdot}3H_2O$, $Ca(HSeO_3)_2{\cdot}H_2O$, $SrSeO_3$, $SrSeO_3{\cdot}2H_2O$, $SrSe_2O_5{\cdot}H_2O$ and $Sr(HSeO_3)_2$ were prepared by normal evaporation or precipitation techniques.

Nilson [27] prepared magnesium selenite hexahydrate by precipitation of magnesium chloride solution with a sodium selenite solution. The thermodynamic properties for the formation of $MgSeO_3{\cdot}6H_2O$ were investigated by Leshchinskaya [28] on the basis of calorimetric measurements.

Ebert and Havlicek [18,23,24] and Yanitskii et al. [25] systematically prepared all selenites in the $MSeO_3$–SeO_2–H_2O system (M = Be, Mg, Ca, Sr) at 298 K and studied their bonding conditions. Neal and McCrosky [29] synthesized barium selenites with regard to their solubility diagram. Several hitherto unknown divalent metal acid selenites were prepared and characterized by IR spectroscopy and X-ray studies [30].

2.3. Synthesis of Al, Ga and In selenites

Morris et al. [31–33] synthesized and determined structures of $Al_2(SeO_3)_3{\cdot}xH_2O$ ($x = 3$, 6) and $AlH(SeO_3)_2$. Gospodinov [34] drew the solubility isotherm of the Al_2O_3–SeO_2–H_2O system at 373 K and reported thermal and X-ray analysis of the products obtained. Gallium hydrogen selenite diselenite hydrate, $Ga(HSeO_3)(Se_2O_5){\cdot}1.07H_2O$, a novel structural type, containing alternate cationic and anionic layers, was prepared hydrothermally and crystal data reported [11]. $InHSe_2O_6$ was prepared hydrothermally and characterized by single crystal X-ray diffraction techniques [35].

The interaction of MCl_3 (M = Al, Ga, In) with Na_2SeO_3 and H_2SeO_3 in aqueous solutions was investigated [36] at a constant initial concentration of $MCl_3 = 0.3\ mol\ l^{-1}$. Depending on the amount of Na_2SeO_3 present, $Al_2(SeO_3)_3{\cdot}6H_2O$, $In_2(SeO_3)_3{\cdot}6H_2O$, $Ga(OH)SeO_3{\cdot}2.5H_2O$ or the products of their hydrolysis precipitate and, in the final stages, the hydroxides or the gallates. Only by hydrothermal crystallisation of gallium selenites from acidic solution of alkali metals, could double selenites of variable composition, $M_xH_{1-x}Ga(SeO_3)2H_2O$ (M = Rb, Cs, and $x = 0.3$–0.8), be isolated [37].

2.4. Synthesis of transition metal selenites

Interest in the synthesis of new transition metal selenites has been increasing during the last few years [11,31,38–49]. Many new solid state materials have been synthesized by hydrothermal reactions [50,51]. This technique is considered to have the potential of producing metastable materials with novel structures and unusual physical properties [52].

2.4.1. Synthesis of Sc, Y and La selenites

When scandium ions react with solutions of selenous acid or alkali metal selenites, two types of hydrogen selenites, $ScH(SeO_3)_2{\cdot}H_2O$ [53] and $Sc(HSeO_3)_3$ [54,55] are formed. Attempts to prepare

Sc compounds in which the proton is replaced by an alkali metal or ammonium ion were unsuccessful, but compounds of this type have been obtained with certain rare-earth elements [56]. The preparation of the amorphous product $NaY(SeO_3)_2 \cdot 3H_2O$ has been reported [57]. Normal [54] and complex scandium selenites have been isolated and studied [58]. They all display low solubility. Lanthanum hydrogen selenite was synthesized hydrothermally and atomic coordinates reported [59].

2.4.2. Synthesis of V, Nb, and Ta selenites

Vanadium selenites reported so far include VSe_2O_6 [60], $VOSeO_3$ [61], $VOSeO_3 \cdot H_2O$ [62], $NH_4(VO)_3(SeO_3)_2$ [63], $K_2V_2SeO_7$ [64] and $Ba(VO)_2(SeO_3)_2(HSeO_3)$ [65]. The last four of these were synthesized from hydrothermal reactions. Hydrothermal reactions in the V_2O_5–SeO_2–AOH systems (A = Na, K, Rb, Cs, NH_4) were studied [66] with various reagent mole ratios. The reactions at 503 K produced single phase products of the general formula $AV_3Se_2O_{12}$ with the $NH_4(VO_3)_3(SeO_3)_2$ structure type. The dependence of the synthesis results on the reaction conditions is discussed and rationalised.

Tantalum selenite has been synthesized [67,68] under various conditions. No niobium selenites have been prepared.

2.4.3. Synthesis of Cr, Mo, and W selenites

Harrison et al. [69] hydrothermally prepared and characterized $Cr_2(SeO_3)_3 \cdot 3H_2O$. Shakhova and Morosanova [70] have investigated molybdenum selenites. The hydrothermal synthesis and crystal structure of $(NH_4)_2(WO_3)_3SeO_3$ and $Cs_2(WO_3)_3SeO_3$, two new non-centrosymmetric, layered tungsten(VI)-containing phases, have been reported [71]. These compounds are isostructural with their molybdenum(VI) containing analogues.

2.4.4. Synthesis of Mn, Tc, and Re selenites

$Mn_2(SeO_3)_3 \cdot 3H_2O$ [72] was crystallized from suspension of freshly precipitated hydrated manganese dioxide and concentrated selenous acid. The crystals were well developed, lustrous and dark brown prisms. Khandelwal and Mallela [73] synthesized and studied new selenite complexes of Mn(II). Manganese(III) complexes have also been prepared [74].

In the course of synthetic experiments in the system MnO_2–SeO_2–H_2O–X_2O (X = Li, Na, K) aimed at the preparation of selenite compounds containing manganese in its tetravalent state, the following new phases have been obtained and investigated: $Mn(SeO_3)_2$ [46,75], $K_2Mn(SeO_3)_2$ [76] and crystals of the new Mn(II)–Mn(III) mixed-valence compounds $Li_5Mn(II)_4Mn(III)(SeO_3)_8$, $KMn(II)_4Mn(III)(SeO_3)_6$ [44] and $Mn(II)Mn(III)_2O(SeO_3)_3$ [45] were synthesized hydrothermally.

No Tc or Re selenites have been reported.

2.4.5. Synthesis of Fe, Ru, and Os selenites

The synthesis and crystal chemistry of iron(III)–selenium(IV) oxo-salts have been the subject of detailed investigations within the last few years; dozens of new phases result therefrom [77–79]. Pinaev and Valkova [80] studied the synthesis of iron(III) selenite at various Fe/SeO_3^{2-} ratios, pHs, temperatures and using different Fe(III) salts. After establishing optimum conditions, a product of composition $Fe_2O_3 \cdot 3.048SeO_2 \cdot 7H_2O$ was obtained which was finely crystalline and paramagnetic. Pinaev et al. [81] prepared light green crystalline $Fe_2O_3 \cdot 4SeO_2 \cdot H_2O$ in an autoclave at 523 K (within 12 to 15 h) from Fe(III) selenite heptahydrate and an aqueous solution of SeO_2.

Most recently, the compounds $Rb_4MFe_4(SeO_3)_{14}(SeO_2OH)_2 \cdot 2H_2O$ (M = Mg,Cu) [82], $KFe_2(SeO_3)_3(SeO_2OH)$ [83] and $NaFe(SeO_3)_2$ [84] were obtained. $ZnFe_2(SeO_3)_4$ [85] was obtained as a coprecipitate of $Zn_3Fe_2(SeO_3)_6$ [79] in the system H_2O–SeO_2–$FeC_2O_4 \cdot 2H_2O$–$ZnSeO_3$ and its crystal structure studied.

As part of a study on Kieserite-type compounds, $M(II)(XO_4) \cdot H_2O$ (M = Mg, Mn, Fe, Co, Ni, Zn; X = S, Se), the precipitation products of H_2SeO_4 reacted with solutions of iron(II) have been examined in the temperature range upto 523 K [85]. Without exception, iron(II) was oxidized, often combined with a (partial) change of the valence state of the Se ions from (VI) to (IV). Several new compounds were found, which encouraged a systematic investigation of iron(III) selenites(IV). It turned out that $FeC_2O_4 \cdot 2H_2O$ (with Fe(II) oxidizing during the synthesis) and SeO_2 were appropriate starting materials for hydrothermal syntheses, using addition of further di- and/or monovalent cations. $M_3Fe_2(SeO_3)_6$ (M = Zn, Cu) crystals were obtained and characterized [79]. The crystals are brownish (Cu), or olive green (Zn). A

study in systems containing iron and selenium led to the synthesis and structural investigations of $Fe_2(SeO_3)\cdot H_2O$ [49], $KFe(SeO_3)_2$ [86], $LiFe(SeO_3)_2$ [87] and $LiFe(Se_2O_5)_2$ [88].

Information on Ru, Os selenites could not be traced.

2.4.6. Synthesis of Co, Ni and platinum group selenites

Dark violet single crystals of $CoSeO_3$-II, in sizes upto 1 mm, were obtained [89] as the main crystalline product, in synthesis experiments aiming at the preparation of Rb analogues of the $K_2Co(SeO_3)_2$, $K_2Co_2(SeO_3)_3$ and $K_2Co_2(SeO_3)_3\cdot 2H_2O$ compounds [90–92]. The presence of Rb ions in the primary solutions seems to have [89] a promotive effect on the formation of $CoSeO_3$ but no detailed investigations on this effect were made. When Rb^+ was omitted in the starting solutions or replaced by chemically related (e.g., K^+, Cs^+) or similarly sized cations (e.g., Ba^{2+}), the formation of $CoSeO_3$-II could not be observed. Dark violet pleochroic single crystals of $Co_3(SeO_3)_3\cdot H_2O$ upto ~0.3 mm and yellow crystals of $Ni_3(SeO_3)_3\cdot H_2O$ upto ~0.2 mm were obtained hydrothermally [93,94].

Wildner [95] synthesized single crystals of $K_2[M_2(SeO_3)_3]\cdot 2H_2O$ (M = Co, Ni) under hydrothermal conditions, from $M(OH)_2$, SeO_2 and K_2CO_3. Their structures were determined using single crystal X-ray data. The investigations confirmed that these represented the first selenites belonging to the zemannite structure type, a framework structure with wide channels, running parallel [0001].

The distorted perovskite-type phase $NiSeO_3$ has been prepared at high temperature and pressure, and orders antiferromagnetically at 98 K [96]. Other nickel selenites include the naturally occurring ahlfeldite, $NiSeO_3\cdot 2H_2O$ [97], which is isomorphous with other hydrated divalent selenites, $MSeO_3\cdot 2H_2O$ (M = Mg, Mn, Co, Cu, Zn), and the diselenite, $NiSe_2O_5\cdot 3H_2O$ [98] which adopts the same structure as its cobalt and zinc analogues. Ebert et al. [99] have carried out IR and thermal measurements on various nickel–selenium–oxygen phases and reported the new phase composition $Ni(HSeO_3)_2\cdot 2H_2O$. McManus et al. [100], in search of new transition metal oxides with unusual physical properties, have produced another hydrated nickel selenite, $Ni_3(SeO_3)_3\cdot H_2O$ (or $NiSeO_3\cdot(1/3)H_2O$) which has been characterized by single crystal X-ray diffraction and TG measurements. Crystals of $Ni_3(SeO_3)_3\cdot H_2O$ were grown hydrothermally. From aqueous solutions of $M(HSeO_3)_2$, single crystals of $Mg(HSeO_3)_2\cdot 4H_2O$ and of the hitherto unknown compounds $M(HSeO_3)_2\cdot 4H_2O$ (M = Co, Ni, Zn) were obtained [30].

Harrison et al. [101] described the synthesis and structure of the phase $CoSe_2O_5$, which is isomorphous with $ZnSe_2O_5$ [40]. Purple transparent crystals of the compound were hydrothermally synthesized from $CoSO_4\cdot 7H_2O$ and excess SeO_2.

Reactions of selenous acid and potassium selenite with potassium chloroplatinite and chloroplatinate were studied by Derbisher [4]. Selenous acid oxidizes chloroplatinite, $PtCl_4^{2-}$ to chloroplatinate, $PtCl_6^{2-}$ in the cold. On heating, the oxidation is more rapid and the yield of large bright yellow crystals of K_2PtCl_6 is greater. In contrast with the reaction of H_2SO_3 with potassium chloroplatinite which leads to the coordination of the SO_3^{2-} group and formation of a sulphite compound [102], H_2SeO_3 does not form a selenite compound with K_2PtCl_4. Selenous acid does not form complex selenites with K_2PtCl_6, either, but catalytically enhances the solubility in water. However, the reaction of potassium selenite with $PtCl_6^{2-}$ produces $K_3[Pt(SeO_3)_2(OH)_3H_2O]\cdot 2H_2O$ and the compound $H[PtSeO_3(OH)_3H_2O]$ was also obtained [4].

No selenite compounds of rhodium, iridium or palladium appear to have been synthesized.

2.4.7. Synthesis of Cu, Ag, and Au selenites

Numerous studies have been devoted to copper selenites [103–108]. At room temperature $CuO–SeO_2–H_2O$ shows [103,105,108] two phases $CuSeO_3(H_2O)_2$ and $Cu(HSeO_3)_2$. Hiltunen et al. [107] reported a crystallographic study of $Cu(HSeO_3)_2(H_2O)$. Lafront and Trombe [109] redetermined its crystal structure and its thermal behaviour showed it to have two water molecules instead of one. However, Micka et al. [106] did not report this phase. The synthesis, thermal stability, and structure of the novel compound $[Cu(HSeO_3)_2(NO_3)_2]2NH_4^+$, NH_4NO_3 was reported [109] and the structural relationships of the reported complexes with $Cu(HSeO_3)_2$ were emphasized. The $Cu(HSeO_3)_2$ phase may be regarded as a layered 'host compound' which can include, in solution according to the pH value, water molecules, ammonium nitrate or other entities [110].

In the presence of chlorides instead of nitrates, a new family of bimetallic hydrogen selenites $[Cu(HSeO_3)3Cu_xM_{1-x}Cl_2(H2O)_4]$ (where M = Mn, Co, Ni, Cu, Zn and x depends mainly on the nature of the second cation M) is obtained [111]. Lafront et al. [110] also report the synthesis, crystal structure and magnetic characterization of this new family.

Gospodinov [111] studied the solubility and reported solubility products of $CuSeO_3$ (1.5×10^{-11}) and Ag_2SeO_3 (1.72×10^{-16}). Markovskii et al. [112] synthesized $Au_2(SeO_3)_3H_2SeO_3$ by treating $Au(OH)_3$ with excess H_2SeO_3.

2.4.8. Synthesis of Zn, Cd, Hg, and Pb selenites

A few zinc selenites have been reported [85]. According to the literature [30,113,114] various cadmium selenites exist as water insoluble fine microscopic needles. The solubility diagrams in the $MSeO_3$–SeO_2–H_2O (M = Zn [115], Cd, Hg [116]) systems at 298 K were studied. These systems can be compared with the systems of the selenites of other divalent metals on the basis of the types of salts formed. The systems of cadmium(II) and mercury(II) selenites are located [117], according to their behaviour, between the systems of zinc(II) and barium(II) selenites and the systems of the other divalent metals. With Cd(II) and Hg(II) an acid salt with a ratio of $n(M^{II})$ to n(Se) of greater than 1 : 2 is formed and, in addition, a condensed salt of Cd(II) – a diselenite. The formation of acid salts with a ratio of $n(M^{II})$ to n(Se) of 1 : 2, found for a number of other divalent metals, can be assumed at lower temperatures. For zinc, this has been confirmed by the formation of $Zn(HSeO_3)_2{\cdot}2H_2O$ in the study of the $ZnSeO_3$–H_2O system at 273 K [116]. So far, the $CdSeO_3$–H_2O system is the only known system, containing selenites, that forms diselenite and an acid salt, simultaneously at a single temperature.

Verma and Khushu [114,118] have prepared and studied Ba, Cd and Pb selenites. Markovskii and Sapozhnikov [119] isolated and studied neutral, acid and diselenites of lead. In addition, a double salt, approximating to $PbSeO_3{\cdot}Pb(NO_3)_2$ was also synthesized.

2.4.9. Synthesis of lanthanide and actinide selenites

Although rare-earth selenites were discovered by Berzelius in 1818 [120], more than a century and a half elapsed before further investigations were reported [121,122]. Considerable efforts have been made to obtain and characterize, in aqueous solutions, new rare-earth hydrated selenites and hydrogen selenites [123]. Of particular interest is the family of rare-earth selenites and hydrogen selenites $LnH(SeO_3)_2{\cdot}nH_2O$, (where Ln = a lanthanide element), on account of their optical and magnetic properties [124–126]. Compounds of Se(IV) [127–129] have been systematically investigated in an attempt to understand their structural chemistry. These compounds have been described as having a layered structure, with groups of hydrogen selenite, selenite, and diselenite such as $LaHSe_2O_6$ [59], $PrH_3(SeO_3)_2(Se_2O_5)$ [130], or hydrated $LnH(SeO_3)_2{\cdot}2.5H_2O$ [126].

Pedro et al. [131] reported the synthesis, characterization, and crystal structure of $Nd(HSeO_3)(SeO_3){\cdot}2H_2O$. A glass was prepared as precursor for the crystal growth of $Nd(HSeO_3)(SeO_3){\cdot}2H_2O$ for pseudo-hydrothermal synthesis, by heating a mixture of SeO_2 and Nd_2O_3 (molar ratio 10 : 1) for 24 h at 723 K in a sealed outgassed Pyrex ampoule, followed by quenching in liquid nitrogen. A sample of the glass, together with water, in a Teflon tube was placed in a tightly closed steel container and maintained at 383 K for a week. After slow cooling light pink crystals were obtained. In a similar manner, Castro et al. [132] synthesized, characterized and solved the crystal structure of $Pr_2(HSeO_3)_2(SeO_3)_2$ (light green crystals). Erbium selenite(IV) selenate(VI) hydrate, $Er(SeO_3)(SeO_4)_{0.5}{\cdot}H_2O$, was prepared hydrothermally and the crystal structure determined [47]. Only two other compounds containing both Se(IV) and Se(VI) oxyanions in the same crystal structure are reported, i.e, $Li_2Cu_3(SeO_3)_2(SeO_4)_2$ [133], and the rare mineral schmiederite, $Pb_2Cu_2(SeO_3)(SeO_4)$ [134]. A compound of this kind has also been postulated in the decomposition of a hydrated lanthanum selenate [135]. Pedro et al. [136] synthesized and characterized 44 novel $R_2Se_aO_{3+2a}$ ($a = 4$; 3.5; 3; 1) compounds, which crystallize in seven different structure types. The anhydrous rare-earth selenites of composition $R_2Se_4O_{11}$ (R = Y, La, Gd, Tb, Dy, Ho, Er, Tm, Yb, Lu) and $R_2Se_{3.5}O_{10}$ (R = Pr, Nd, Sm, Eu, Gd, Tb) were prepared by solid state reactions between stoichiometric mixtures of analytical grade R_2O_3 (R = Y, La, Nd, Sm, Eu, Gd, Dy, Ho, Er, Tm, Yb, Lu), Pr_6O_{11} or Tb_4O_7, with SeO_2. Reactants were ground before

heating in evacuated Pyrex ampoules at 688 K for 36 h, and then quenched in liquid nitrogen. All the products were isolated as white or pale-colored polycrystalline powders (Nd, blue; Er, pink).

Claude [137] and Khandelwal and Verma [138] synthesized and studied UO_2SeO_3 and its ammonium and potassium complexes. Uranyl hydroxo selenite and its derivatives have also been reported [139]. Verma and Khandelwal [140] studied the behaviour of H_2SeO_3 towards uranyl acetate solution conductomerically.

3. Thermal studies

3.1. Thermal behaviour of alkali metal selenites

The thermal stability of crystalline $LiHSeO_3$ and $LiH_3(SeO_3)_2$ has been studied [141] by chemical and X-ray phase analysis. The acid salt is initially converted to stable $Li_2Se_2O_5$, which is converted, on further heating, to Li_2SeO_3. The transition temperatures were 378 and 651 K. The m.p. of $Li_2Se_2O_5$ is 453 K and that of Li_2SeO_3 903 K. Itoh et al. [142] studied the thermal decomposition of ferroelectric lithium trihydrogen selenite, $LiH_3(SeO_3)_2$. It transforms from a crystalline to amorphous state at 353 K. The transformation is endothermic and there is a decrease in mass. The X-ray halo intensity gradually develops above the transition temperature, at the expense of the Bragg diffraction intensity. The surface transformation originates from the decomposition having a long characteristic time.

The curve obtained [143] from the DTA of $NaHSeO_3$ has four endothermic regions with maxima at 387, 616, 818 and 903 K. TG, chemical and X-ray analysis allowed the steps to be ascribed to:

1. $2NaHSeO_3 \rightarrow Na_2Se_2O_5 + H_2O$
2. melting of $Na_2Se_2O_5$
3. $Na_2Se_2O_5 \rightarrow Na_2SeO_3 + SeO_2$
4. melting of Na_2SeO_3 with partial decomposition.

The DTA curves of $NaH_3(SeO_3)_2$ have maxima at 387, 623, 881, and 983 K. The first maximum corresponds to

$$2NaHSeO_3 \cdot H_2SeO_3 \rightarrow Na_2Se_2O_5 + 2SeO_2 + 3H_2O$$

and maxima 2–4 are attributed [143] to the same processes as found for $NaHSeO_3$. Decomposition products of both salts heated to 1373 K are composed mainly of Na_2O.

Thermal analysis of K_2SeO_3, at temperatures upto 875 K, revealed that only evaporation of moisture (the compound being strongly hygroscopic) and a polymorphic change occurred [14]. In contrast to some studies [144,145], neither decomposition nor successive oxidation of the sample to selenate was observed.

Thermal decomposition of $KHSeO_3$ (375 to 420 K) is characterized by the transition to diselenite

$$2KHSeO_3 \rightarrow K_2Se_2O_5 + H_2O$$

Similar processes, connected with incongruent melting of hygroscopic substances, were observed [146] for all the acid alkali-metal selenites of the $MHSeO_3$ type. The effect of the hydrogen bond strength on the decomposition temperatures can be followed if the behaviour of the deformation vibrations of the hydroxyl groups, δ(OH), is used as a criterion of the strength of the hydrogen bond system [14]. The lowest wave number found in the spectra for the alkali metal compounds was for $KHSeO_3$ and corresponded to the longest hydrogen bond [147] and to the lowest temperature of decomposition of the compound to diselenite. Thus, the lowest temperature of the transition of hydrogen selenite to diselenite for heterogeneous M_2SeO_3–H_2SeO_3–H_2O systems was found for potassium compounds.

The initial process of thermal decomposition of $KH_3(SeO_3)_2$ (298 to 465 K) can be described [14] by

$$2KH_3(SeO_3)_2 \rightarrow K_2Se_2O_5 + 2SeO_2 + 3H_2O$$

The compound first melts incongruently, with evaporation of the released water accompanied by two endothermic effects. The DTA effect corresponding to a polymorphic change of $K_2Se_2O_5$ is overlapped by a strong endothermic effect accompanying sublimation of released SeO_2. Because the sublimation was not complete before the beginning of the diselenite decomposition, the TG curve did not exhibit a plateau for this substance alone. Nevertheless, a plateau appears on the decomposition curve at higher temperatures. This demonstrates that pure diselenite can be prepared by thermal decomposition of $KH_3(SeO_3)_2$.

Thermal behaviour of $K_5H_3(SeO_3)_4$, in its initial phase, can be described [14] by

$$2K_5H_3(SeO_3)_4 \rightarrow 5K_2SeO_3 \cdot 3SeO_2 + 3H_2O$$

During further heating, the intermediate product decomposed to selenite and Se(IV) oxide and there was some partial oxidation to selenate. The thermoanalytical properties of the potassium selenites studied [14] could be explained using the method of gradually increasing temperature. In contrast to thermogravimetry, this procedure allows for a distinct recording of all intermediate products.

It has been reported [148] that rubidium selenite is converted into the selenate at 673 K. DTA of Rb_2SeO_3 shows [149] two endothermic effects, a weak effect at 453 K and a larger effect at 1263 K and three exotherms at 583, 613 and 763 K. At about 453 K, in air, a very small amount of Rb_2SeO_3 undergoes disproportionation with formation of elemental selenium. At about 583 K, stepwise oxidation begins and leads to the formation of a product whose composition corresponds to the formula $Rb_2SeO_3{\cdot}3Rb_2SeO_4$. The product melts at 1263 K without decomposition.

The weakest ferroelectric $RbD_3(SeO_3)_2$, as distinguished from $RbH_3(SeO_3)_2$ crystals, after the lock-in phase transformation from incommensurate to commensurate phase, has triclinic symmetry [150]. A theoretical group analysis of this effect is given.

The effect of heat on crystalline $Cs_2SeO_3{\cdot}H_2O$ (up to 1273 K) has been studied [151] by DTA, TG, X-ray diffraction, crystal-optical, and chemical methods. When the salt is heated in air, the following changes take place: (i) at 373 to 403 K, 0.5 mol of water and about 0.05 mol of CsOH (per mol of the original salt) are lost, (ii) at 483 K, dehydration is completed, (iii) a further 0.05 mol of CsOH is volatilised, and SeO_2 disproportionates with the formation of 0.02 g-atom of Se, at 603 K and (iv) at 713 K, selenite is oxidised with the formation of a product $Cs_2SeO_3{\cdot}Cs_2SeO_4$, which is stable until fusion takes place. Fusion (at 1033 K) is accompanied by the almost complete oxidation of the product to Cs_2SeO_4. When heated out of contact with air or in an inert atmosphere, $Cs_2SeO_3{\cdot}H_2O$ loses water, a small quantity of CsOH and free selenium, with the formation of a small quantity of SeO_2 by disproportionation. Almost no oxidation of selenite is observed under these conditions.

Comparison of the behaviour of various alkali metal selenites on heating shows that disproportionation (with formation of elemental selenium) is characteristic mainly of the hygroscopic K, Rb, and Cs salts, while the nonhygroscopic Li and Na selenites hardly disproportionate at all [152]. Anhydrous and hydrated ammonium selenites decompose to form water ammonia and ammonium diselenite [153] in the temperature range 305–355 K. Similarly, the first intermediate in the decomposition of ammonium hydrogen selenite is ammonium diselinite, formed in the temperature range 300–315 K with liberation of water. Further decomposition of diselenite occurs from 355 to 425 K with formation of ammonia and yields the strongly hygroscopic, X-ray amorphous compound $(NH_4)HSe_2O_5$, which decomposes further according to the reaction

$$4(NH_4)HSe_2O_5 \rightarrow 2N_2 + 10H_2O + 5SeO_2 + 3Se$$

In contrast to the decomposition products of ammonium selenite, the acid selenites of the alkali metals [146] always decompose to yield the corresponding diselenites, which, on further heating, convert to selenites with partial oxidation to selenates.

3.2. *Thermal behaviour of normal alkaline earth metal selenites*

The thermal decomposition of $MgSeO_3{\cdot}6H_2O$ has been studied [23,26,29]. Leshchinskaya and Selivanova [28] obtained amorphous $MgSeO_3$ at 473 K; whereas 328–358 K is the dehydration range [23,26] accompanied by an endotherm. $MgSeO_3$ crystallizes [23] from 673 to 693 K with an exothermic effect. Finally the selenite decomposes

$$MSeO_3 \rightarrow MO + SeO_2 \quad (M = Mg, Ca)$$

$SrSeO_3$ and $BaSeO_3$ do not decompose [26] below 1273 K but instead there is a slight oxidation to selenate above 973 K, which was also confirmed by IR spectra. However, Verma and Khushu [118] while studying $BaSeO_3{\cdot}2.5H_2O$ observed that the anhydrous compound undergoes slight oxidation from 1033 to 1203 K, and then commences decomposition, which continues even beyond 1273 K.

$CaSeO_3{\cdot}H_2O$ dehydrates [18,26] from 408 to 533 K with an endotherm. Thermal analysis of $CaSeO_3$ and X-ray powder diagrams suggest that anhydrous crystalline calcium selenite(I) is formed from 408 to 488 K

which recrystallises between 833 to 843 K to form another crystalline modification of anhydrous calcium selenite(II), and this phase change is endothermic.

Thermal decomposition of $SrSeO_3 \cdot nH_2O$ leads to the formation [83] of the crystal modification $SrSeO_3$(I), which from 613 to 628 K is transformed into the second, as yet not described, modification, $SrSeO_3$(II). $BaSeO_3$ is thermally stable [83] upto 783 K, where it starts partially oxidizing to selenate. This temperature is 140–150 K lower than reported [118,154].

3.3. Thermal behaviour of alkaline earth metal hydrogen selenites

Table 1 summarizes the thermal behaviour of hydrogen selenites. The initial reactants and the products of thermal decomposition were studied [18,23,26] by X-ray diffraction. The dehyrated hydrogen selenites decomposed to diselenites and water

$$M(HSeO_3)_2 \rightarrow MSe_2O_5 + H_2O$$
$$(M = Mg, Ca, Sr, Ba)$$

Further heating decomposes diselenites to normal selenites and selenium dioxide. Finally normal selenites transform to their metal oxides and selenium dioxide

$$MSeO_3 \rightarrow MO + SeO_2 \quad (M = Mg, Ca)$$

The double endotherm from 238 to 350 K and 368 to 378 K in the thermal analysis of $Mg(HSeO_3)_2 \cdot 4H_2O$ indicates [23] the presence of a dehydration intermediate, which could be anhydrous $Mg(HSeO_3)_2$ or a

Table 1
Thermal decompositon of alkaline earth metal hydrogen selenites

Compound	Temperature range (K)	TG mass loss%	DTA	Assignment	Ref.
$Mg(HSeO_3)_2 \cdot 3H_2O$	363–473	16.6	–	dehydration	
	473–558	4.9	–	$MgSe_2O_5$	[26]
	558–773	33.1	–	$MgSeO_3$	
	873–1083	32.8	–	MgO	
$Mg(HSeO_3)_2 \cdot 4H_2O$	338–378	25.0 combined loss	double endo	dehydration	
	423–623	–	$MgSe_2O_5$		
	583–603	–	exo(weak)	?	[23]
	673–723	58.8	endo	loss of SeO_2	
	733 and higher	–	–	$MgSeO_3$ anhydrous crystal	
$Ca(HSeO_3)_2 \cdot H_2O$	353–363	decrease	endo	partial dehydration	
	373–403	8.86	–	?	
	418–403	decrease	double endo	total dehydration	
	528–593	12.0 delay	–	$CaSe_2O_5$	[18]
	603–638	decrease	endo	partial loss of SeO_2	
	653	29.9 delay	–	$Ca_2Se_3O_8$	
	688–733	decrease	endo	loss of rest of SeO_2	
	733 and beyond	46.9 delay	–	$CaSeO_3$ anhydrous crystal II	
$Ca(HSeO_3)_2 \cdot H_2O$	398–533	11.6	–	dehydration and $CaSe_2O_5$ formation	
	533–778	35.0	–	$CaSeO_3$ formation	
$Sr(HSeO_3)_2$	488–548	6.0	–	$SrSe_2O_5$ formation	[26]
	548–748	31.8	–	$SrSeO_3$ formation	
$Ba(HSeO_3)_2$	378–438	4.3	–	$BaSe_2O_5$ formation	
	630–718	28.1	–	$BaSeO_3$ formation	

lower hydrate. Raman measurements under quasistatic heating conditions also showed [155] the intermediate formation of anhydrous selenite.

The only possible explanation [18] of the complicated thermal decomposition, Table 1, of calcium hydrogen selenite is based on the assumption of inequality of the position occupied by the $HSeO_3$ ion in the crystal structure of the hydrogen selenite. The water of constitution and hydration is set free, during formation of diselenite ions, more readily from one half of these positions than from the other half. The conversion of diselenite to selenite proceeds analogously. SeO_2 is set free more readily from one half of the positions than from the other, therefore, the intermediate product, $Ca_2Se_3O_8$ can be isolated. The IR spectrum of $Ca_2Se_3O_8$ [18] suggests that Se–O–Se bonds are present in the structure and it is possible, with respect to the width of the intensity of stretching vibrations of the Se–O bond, that the mentioned structure contains both SeO_2 and SeO_3 groups in accordance with the concept mentioned above. Losoi and Valkonen [26], however, do not appear to have isolated $Ca_2Se_3O_8$ during the pyrolysis of calcium hydrogenselenite (Table 1).

$Sr(HSeO_3)_2$ dehydrates [26] to $SrSe_2O_5$ in the temperature range of 488 to 548 K. The diselenite transforms to $SrSeO_3$ from 548 to 748 K. The temperatures reported by Ebert and Havlicek [24] for these two changes are 453–633 K and 453–693 K, respectively.

3.4. Thermal behaviour of Zn, Cd, Hg, and Pb selenites

3.4.1. Thermal behaviour of zinc selenites

According to some authors [156,157], the dehydration of $ZnSeO_3 \cdot 2H_2O$ takes place in two stages with the formation of the intermediate monohydrate. The latter loses water to give the α-modification of anhydrous $ZnSeO_3$, which on further heating is converted into the stable β-$ZnSeO_3$. This form melts at 893 K and is completely dissociated to ZnO at 933 to 973 K and atmospheric pressure. The nature of the dehydration of zinc selenite dihydrate depends [158] to a considerable extent on the conditions of the reaction, and particularly on the external pressure. The dehydration curves in air and with continuous evacuation at a pressure of 10^{-2} mm Hg are shown in Fig. 1. The

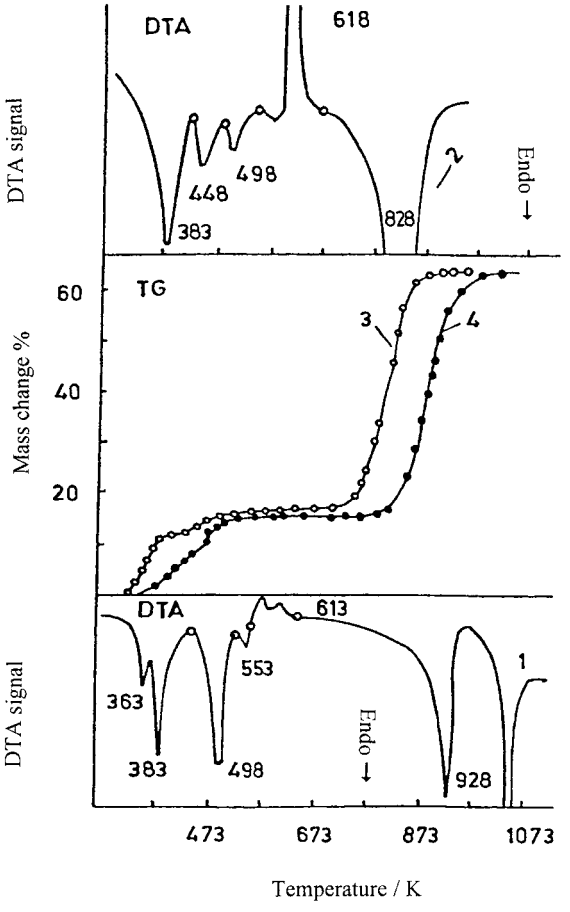

Fig. 1. Differential thermal analysis (DTA) and thermogravimetric (TG) curves obtained by heating $ZnSeO_3 \cdot 2H_2O$ at atmospheric pressure (1,4) and in a vacuum (2,3). Adapted from [158].

low temperature regions of the DTA curves of the coarsely crystalline specimens sometimes show additional peaks. The curves obtained by heating in a vacuum, or by heating finely ground specimens at atmospheric pressure, are independent of the type of specimen. The point of inflection on the TG curve depends on pressure, from about 8% at atmospheric pressure, which corresponds formally to the removal of 1 mol of water, to about 12% on evacuation. The final mass loss on dehydration (16%) corresponds to practically stoichiometric dehydration of the dihydrate. The more complex course of the dehydration compared with the simple two-stage process is also indicated by the DTA curves which show a series of endothermic effects with minima at 363, 383, 498 and

533 K at atmospheric pressure and at 383, 448 and 498 K in a vacuum, Fig. 1. On further heating of the sample, the section of curves in which there is no mass loss shows exothermic transformations at 578 and 613 K (618 K in a vacuum). Subsequently, anhydrous zinc selenite melts at 928 K and decomposes to zinc oxide at 1043 K. In a vacuum, it dissociates before the melting point (minimum on the DTA curve at 828 K).

The differential thermobarometric analysis (DTBA, Fig. 2) curves for the removal of water confirm that the dehydration is a complex process. A remarkable feature is that the specimen, dehydrated under isothermal conditions as far as a mass loss corresponding to the formation of the monohydrate, shows a number of effects, and the curve corresponds, approximately, to the dehydration of the monohydrate only at mass losses greater than 12%, to which the effect at 498 K can be assigned, because, for the monohydrate, temperatures of dehydration coincide with those for the pure phases [159].

Experiments indicate [158] that the dehydration of zinc selenite dihydrate takes place by two simultaneous processes

$$\nearrow ZnSeO_3.H_2O \rightarrow \alpha\text{-}ZnSeO_3 \rightarrow \beta ZnSeO_3 \quad (a)$$

$$ZnSeO_3.2H_2O$$

$$\searrow ZnSeO_3 .x\ H_2O \rightarrow ZnSeO_3(x\text{-}y)H_2O \rightarrow ZnSeO_3(amorph)\beta\text{-}ZnSeO_3 \quad (b)$$

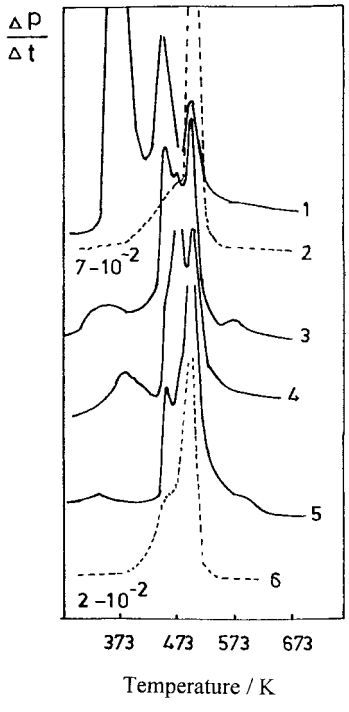

Fig. 2. Differential thermobarometric curves (DTBA) for $ZnSeO_3{\cdot}2H_2O$ (1) and $ZnSeO_3{\cdot}H_2O$ (2) specimens obtained by dehydrating $ZnSeO_3{\cdot}2H_2O$ under isothermal conditions at atmospheric pressure to $\Delta m = 8.55\%$ (4) and in a vacuum to $\Delta m = 8.00\%$ (3) and to $\Delta m = 11.80\%$ (5). Curve (6) is for a specimen heated under the conditions of the thermographic experiment to 423 K. Adapted from [159].

At atmospheric pressure, the reaction takes place chiefly by route (a), but with a decrease in pressure, the proportion of products formed by route (b) increases. The presence of an amorphous phase of variable composition in the intermediate dehydration products is indicated by comparison of the observed degrees of transformation with the results of the thermal analysis and the behaviour of the paramagnetic traces during dehydration. It is significant that, in spite of the observed complexity of the dehydration, the loss of water is stoichiometric, unlike that of the analogous compounds of cobalt, nickel and copper. This agrees with the lower energy of the hydrogen bond in zinc selenite hydrates and the correspondingly lower probability of removal of a proton from the water molecule, and with the absence, according to PMR data [158] of isolated protons in these hydrates as products of the dissociation of coordinated water. In agreement with this, hydrolytic splitting of zinc selenite is not observed on dehydration of its hydrates. Moreover, comparison of the thermal dehydration in the series of selenite dihydrates of the d^5–d^{10} elements of the same type shows that, in the aquo-complexes containing firmly bound water molecules, the composition and state of the intermediate products are determined not so much by the structural nonequivalence of the water molecules as by the energy and mode of their interaction with surrounding species.

DTA and TG curves of $Zn(HSeO_3)_2{\cdot}4H_2O$ indicate [155] that thermal decomposition results in the

direct formation of $ZnSe_2O_5$. However, Raman heating spectra, under quasi-static conditions, show the formation of intermediate anhydrous hydrogen selenite.

3.4.2. Thermal behaviour of Cd, Hg, and Pb selenites

The thermal stabilities of zinc and cadmium selenates and selenites are of interest [160] in connection with the manufacture of phosphors, glass, and in the study of oxidation of zinc and cadmium selenites. The thermal behaviour of cadmium selenites has been studied by several investigators [114,117,161,162]. The heating curves for specimens of $CdSeO_3$, phase I or phase II, show two endothermic effects at 943 to 953 K corresponding to fusion of the salt, and an indistinct effect corresponding to dissociation of the salt with evolution of SeO_2 [114]. This begins at 1013 K and is complete at about 1273 K. However, Micka et al. [117] and Verma and Khushu [161] observed partial decomposition of $CdSeO_3$ upto 1273 K.

The heating curves of $3CdSeO_3 \cdot H_2SeO_3$, Fig. 3, show four endothermic effects (i) an effect at 486 ± 10 K corresponding to removal of 1 mol of water and conversion to $3CdSeO_3 \cdot SeO_2$; (ii) an effect at 668 ± 10 K, for the removal of 1 mol of selenium dioxide; (iii) a reversible effect at 950 ± 10 K, corresponding to fusion of the $CdSeO_3$ (phase I) formed; and (iv) an indistinct effect at 1123 to 1273 K, corresponding to dissociation of the neutral cadmium selenite.

Analysis of the infrared spectra and thermoanalytical curves [117] confirmed that the compounds formed in the system $CdSeO_3$–SeO_2–H_2O are cadmium(II) diselenite, $CdSe_2O_5$ and cadmium dihydrogen tetrakis (selenite) $Cd_3H_2(SeO_3)_4$. $CdSe_2O_5$ decomposes endothermally to $CdSeO_3$ with loss of SeO_2 in the temperature range 565–665 K.

In the temperature range 405–595 K, mercury(II) selenite decomposes only partly [117]. Complete decomposition at higher temperatures, is accompanied by formation of volatile products (mass decrease of 99.9%). Decomposition of $Cd_3H_2(SeO_3)_4$ and $Hg_3H_2(SeO_3)_4$ in the temperature ranges 485–555 K and 420–480 K, respectively, leads to formation of the corresponding tetraselenites, $M_3^{II}Se_4O_{11}$ and water. The mass decrease in this decomposition is greater

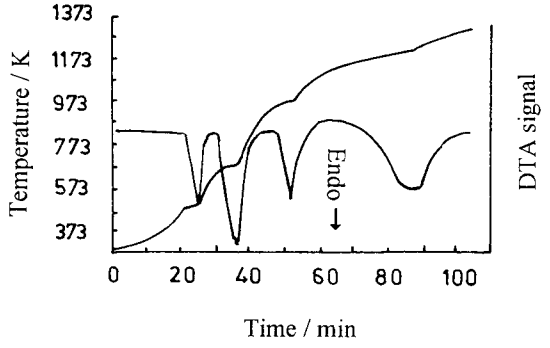

Fig. 3. Heating curve for the acid salt of composition $3CdSeO_3 \cdot H_2SeO_3$. Adapted from [117].

than predicted by theoretical calculations in both cases, because the loss of water is accompanied by partial decomposition and partial loss of SeO_2. For this reason, pure tetraselenites $Cd_3Se_4O_{11}$ and $Hg_3Se_4O_{11}$, cannot be prepared by thermal decomposition of the acid salts. The intermediates, $Cd_3Se_4O_{11}$ and $Hg_3Se_4O_{11}$, decompose further to selenites with loss of selenium dioxide. Gospodinov and Barkov [163] studied the HgO–SeO_2–H_2O system. The crystalline solid phases in equilibrium were obtained in a pure state, and were characterized by chemical, X-ray, crystal-optical and thermal analysis. The mechanism of thermal dissociation of the solid compounds is discussed.

There are two endothermic effects [120] in the $PbSeO_3$ curves. One at 948 ± 10 K, corresponding to fusion of the salt, and a less well-defined one at 1063–1103 K, arising from dissociation of $PbSeO_3$ and evolution of SeO_2, which is complete around 1173–1223 K. Verma and Khushu [161], while studying $PbSeO_3 \cdot 2H_2O$, observed the endotherm at 925 K, corresponding to dehydration. The selenite dissociated completely to PbO by 1203 K. Further loss in mass upto 1273 K is attributed [164] to evaporation of PbO.

The heating curves for the acid salt, $Pb(HSeO_3)_2$, show [120] an endothermic decomposition at 383–393 K. The anhydrous diselenite, $PbSe_2O_5$, begins to decompose at 653 ± 10 K, giving SeO_2, in almost the theoretical amount, upto 713 K. The formation of a $PbSe_2O_5$ phase and its conversion to $PbSeO_3$ on heating to 773 K were confirmed by chemical and X-ray analysis.

3.5. Thermal behaviour of Al selenites

TG curves of $Al_2(SeO_3)_3 \cdot 6H_2O$ showed [165] a steady mass loss, corresponding to the loss of 6 mol of water at about 463 K, followed by loss of SeO_2 to leave a residual solid, which could be formulated as Al_4SeO_8. This residual powder was found to be amorphous by powder XRD. $AlH(SeO_3)_2 \cdot 2H_2O$ loses [165] 2 mol of water at about 523 K. Further mass loss also corresponds to the final compound, Al_4SeO_8.

3.6. Thermal behaviour of transition metal selenites

3.6.1. Thermal behaviour of scandium selenites

Basic scandium selenite, $Sc_2O(SeO_3)_2 \cdot 3H_2O$ has a polymeric structure, in which the bridging entities are oxygen atoms and, apparently, SeO_3 groups. It is insoluble in water and amorphous towards X-rays. In the formation of polymeric scandium groups, with the participation of oxygen and SeO_3 groups, the basic selenites are analogous to the basic carbonates [166]. Water, probably, does not take part in the formation of the structure and is readily removed [55] in a single stage in the temperature range 333–393 K, Fig. 4. The resulting oxide selenite, $Sc_2O(SeO_3)_2$, is an amorphous solid stable upto 723 K. With further increase in temperature, endothermic partial decomposition occurs at 853 K with the removal of 1 mol of SeO_2 and the formation of a new phase – a selenite with the composition $Sc_2O_2SeO_3$. This compound has limited thermal stability and decomposes endothermally at 993 K to scandium oxide.

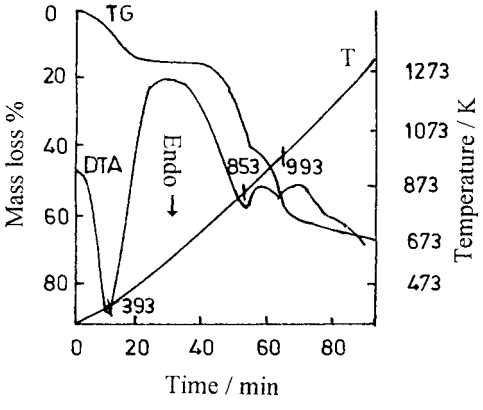

Fig. 4. Thermal curves of $Sc_2O(SeO_3)_2 \cdot 3H_2O$. Adapted from [55].

The thermal decomposition of the normal scandium selenite, $Sc_2(SeO_3)_3 \cdot 5H_2O$, takes place in the range 293 to 1273 K. Reactions in air and in an inert atmosphere N_2, are similar [54], but the temperatures of the endotherms are somewhat increased (about 30 K) in nitrogen. Dehydration of $Sc_2(SeO_3)_3 \cdot 5H_2O$ occurs in a single stage at 393 to 433 K. Anhydrous scandium selenite so formed is amorphous to X-rays and stable upto 673 K. Above 693 K there is stepwise loss of selenium dioxide and, like most of the rare-earth selenites [54], an amorphous intermediate scandium oxide selenite, $Sc_2O_2SeO_3$, is formed. The final decomposition product is scandium oxide, Sc_2O_3.

The DTA curve of scandium hydrogen selenite, Fig. 5 is characterised [54] by several endotherms due to the break down of the substance and the loss of the volatile products, H_2O and SeO_2. The curves are similar, whether recorded in air or in N_2. Water is lost in two stages at 443–463 K and 523–543 K. XRD shows that the dehydrated compound, $Sc_2(SeO_3)_3 \cdot 3SeO_2$, has a [54] different structure from that of the acid selenite. It is stable upto 673 K, beyond which there is loss of SeO_2. Interestingly, half of the selenium present in $Sc(HSeO_3)_3$ is lost at 723–783 K, and crystalline anhydrous normal scandium selenite is formed [54].

It is noteworthy that when either $Sc_2(SeO_3)_3 \cdot 5H_2O$ or $Sc(HSeO_3)_3$ is heated in the range 473–873 K, there is slight reduction of Se^{4+} to red elemental selenium and yellow-orange intermediate products. In composition and properties scandium selenites are analogous to those of rare-earth elements, aluminium, and indium [36].

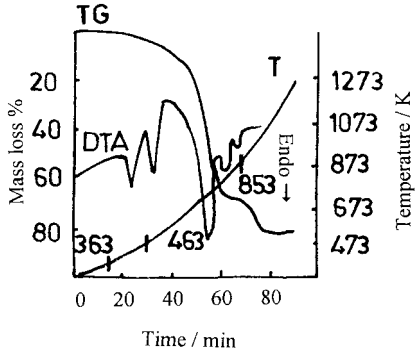

Fig. 5. Heating curves for $Sc(HSeO_3)_3$, heating rate 8–10 K min^{-1}. Adapted from [54].

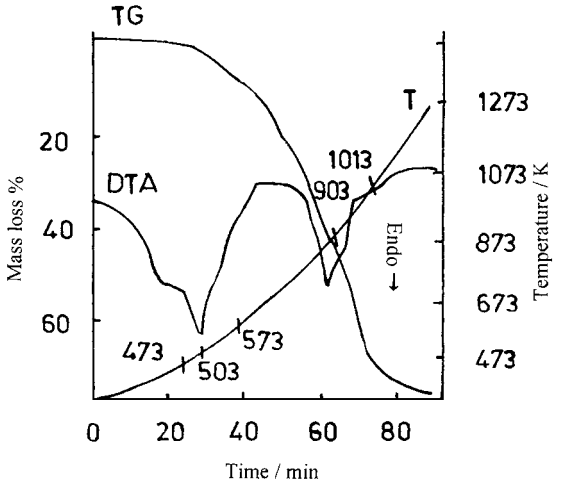

Fig. 6. Thermal curves of $Sc(HSeO_3)_2 \cdot H_2O$. Adapted from [55].

Scandium hydrogen selenite monohydrate, $ScH(SeO_3)_2 \cdot H_2O$, is stable and remains unchanged [55] upto 453 K. Dehydration (473 to 513 K) is accompanied by a change in crystal structure, Fig. 6. Above 573 K decomposition occurs with the complete removal of water and partial, stepwise removal of SeO_2 and the formation of amorphous oxide selenites. At 993 to 1013 K the rest of the SeO_2 is lost and the final product is scandium oxide.

The properties of the complex scandium hydrogen diselenite (above) differ significantly from those of the familiar hydrogen triselenite, $Sc(HSeO_3)_3$. The latter and its monohydrate, have a high stability, apparently, due to the characteristic features of their structures [55]. The last traces of Se from all the scandium selenite decomposition products are removed [58,59] with difficulty only above 1373 K. Khandelwal and Verma had similar difficulty in removing traces of Se from the decomposition products of the potassium derivative of uranyl selenite complexes [138].

3.6.2. Thermal behaviour of vanadium selenites

Kwon et al. [66] performed thermal studies on $AV_3Se_2O_{12}$ (A = K, Rb, Cs, NH_4) and $AVSeO_5$ (A = Rb, Cs) under a flow of N_2 upto 873 K. The % mass changes (either due to SeO_2 or $SeO_2 + NH_3$ loss) and the decomposition temperature ranges for each compound are given in Table 2.

Table 2
Thermal decomposition of vanadium selenites [66]

Compound	Temperature range (K)	Mass change %	
		Observed	Calculated
$AV_3Se_2O_{12}$ series			
A = K	615–698	41.1	41.0
A = Rb	644–697	37.6	37.7
A = Cs	658–701	34.7	34.9
A = NH_4	377–729	46.3	45.9
$AVSeO_5$ series			
A = Rb	655–813	36.6	37.6
A = Cs	663–790	31.6	32.4

3.6.3. Thermal behaviour of Cr, Mo, and W selenites

The TG data for $Cr_2(SeO_3)_3 \cdot 3H_2O$ show [35] the presence of one metastable intermediate phase. At about 673 K the three water molecules are lost, resulting in $Cr_2(SeO_3)_3$. Like the metastable phase of the corresponding indium compound, the remaining Se is lost as SeO_2, over a broad temperature range, to result in Cr_2O_3 by 723 K. Powder X-ray measurements on samples of $Cr_2(SeO_3)_3 \cdot 3H_2O$, heated at 673 K, indicated that the intermediate phase was amorphous.

TG, IR, Raman and X-ray powder data of $M_2(MoO_3)_2SeO_3$ (M = NH_4, Cs) have been presented and discussed [10]. TG curves for $(NH_4)_2(WO_3)_3SeO_3$ showed [8] a two-step mass loss at about 623 and 723 K. The overall mass loss of 18.9% correlated well with the expected 19.0% for complete elimination of H_2O, NH_3 and SeO_2 leaving a residue of hexagonal WO_3 [8]. Further heating to 823 K, under N_2, converted this metastable phase to triclinic WO_3 [8]. A TG run, carried out under flowing oxygen, resulted [8] in a mixture of hexagonal WO_3 and triclinic WO_3 at 723 K.

TG showed [8] that $Cs_2(WO_3)_3SeO_3$ lost 10.4% of its mass in one step between 773 and 873 K. The expected mass loss for sublimation of all the Se (as SeO_2) is 10.2%. The off-white TG residue consists of $Cs_2W_3O_{10}$, of unknown structure [8].

3.6.4. Thermal behaviour of manganese selenites

The dehydration of manganese selenite dihydrate, like that of zinc selenite dihydrate, depends [158] to a considerable extent on the conditions of the reaction and, particularly, on the external pressure. The dehydration curves in air and with continuous evacuation

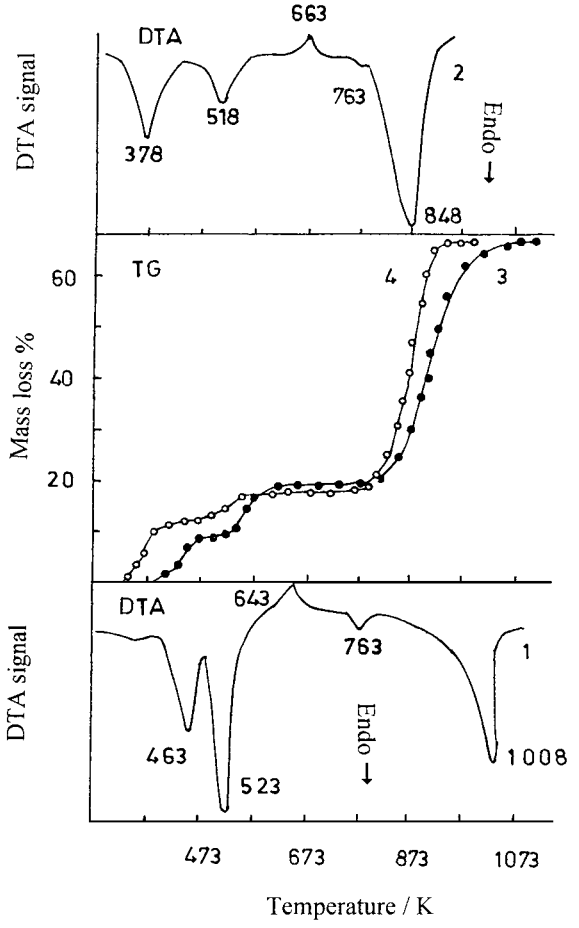

Fig. 7. DTA and TG curves obtained by heating $MnSeO_3 \cdot 2H_2O$ at atmospheric pressure (1,3) and in a vacuum (2,4). Adapted from [158].

are given in Figs. 7 and 2. The final mass loss on dehydration, 17.0%, corresponds to practically stoichiometric dehydration of the dihydrate. The DTA shows endotherms at 463 K and 518 K in vacuum. On further heating, exothermic structural transformations (no mass loss) were observed at 643 K in air, or 663 K in vacuum. Anhydrous manganese selenite dissociates in air to Mn_2O_3 (endotherm at 1008 K) without melting. In vacuum the temperature of dissociation is lowered to 848 K and the solid residue is Mn_3O_4, while a mixture of SeO_2 and elemental Se is evolved as a consequence of the oxidation of Mn^{2+} by the selenium dioxide liberated.

The thermal decompositions of manganese(III) selenites [167] and manganese(III) selenite complexes [168] have been studied. Thermoanalytical results of manganese(III) selenites and the proposed decomposition processes are summarized in Table 3. All compounds lose water only above 413 K, except compound (4), Table 3, where half a mol is lost at 353 K. IR spectra of compounds heated at 473 K to a constant mass showed the absence of water. The decomposition of manganese(III) hydrogen selenite closely resembles that of iron(III) hydrogen selenite [81]. In the case of ammonium diselenite manganese(III), the loss in the range 553–653 K corresponds to the elimination of ammonia, which is confirmed by the IR spectra of heated samples. A significant mass loss around 673 K in all the compounds indicates the formation of manganese(III) oxyselenite. The decompositions of anhydrides to oxyselenites clearly indicates the transient existence of intermediates, as is evident from slight inflexion points instead of horizontal levels in the TG curves. The corresponding DTA peaks show the endothermic effects during the decomposition. Between 713 and 893 K, manganese(III) oxyselenite, except in the case of compound (4) Table 3, is converted to Mn_2O_3. The endothermic peak at the corresponding temperature is associated with this change.

The thermal behaviour of potassium diselenito manganese(III) sesquihydrate, $KMn(SeO_3)_2 \cdot 1.5H_2O$, Table 3, is somewhat different from that of the other compounds. Besides showing endothermic peaks for the loss of water and the formation of oxyselenite, it shows an exothermic effect at 613 K, without any mass loss. This has been attributed to structural transformation [167]. The oxyselenite in this case appears to decompose above 753 K and the mass loss at 913 K corresponds to the formation of manganese(III) dioxyselenite which is not observed in other compounds. The formation of dioxyselenite has, however been, observed [54,169,170] during the thermal decomposition of rare-earth selenites. On further heating to 1113 K the dioxyselenite decomposes to Mn_2O_3.

The effective magnetic moments of the four compounds listed in Table 3, measured at room temperature [167,168], correspond to the value of 4.9 Bohr Magneton required for a high spin d^4 ion without orbital contribution. This clearly confirms the trivalent state of manganese in all the compounds.

Thermoanalytical results for rubidium diselenitomanganese(III) sesquihydrate, $RbMn(SeO_3)_2 \cdot 1.5H_2O$,

Table 3
Thermoanalytical results of manganese(III) selenites [167]

Dehydration/decomposition transition	Temperature (K)		Loss (%)	
	TG	DTA	Calculated	Observed
1. $Mn_2(SeO_3)_3 \cdot 4H_2O$				
$Mn_2(SeO_3)_3 \cdot 4H_2O \rightarrow Mn_2(SeO_3)_3$	413–533	388 endo 563 endo	12.7	12.0
$Mn_2(SeO_3)_3 \rightarrow Mn_2O(SeO_3)_2$	573–713	703 endo	32.5	34.0
$Mn_2O(SeO_3)_2 \rightarrow Mn_2O_3$	713–893	803 endo	71.9	73.0
2. $MnH(SeO_3)_2$				
$2MnH(SeO_3)_2 \rightarrow Mn_2(SeO_3)_3SeO_2$	433–483	488 endo	2.9	3.8
$Mn_2(SeO_3)_3SeO_2 \rightarrow Mn_2O(SeO_3)_2$	493–713	663 endo 713 endo	38.7	41.6
$Mn_2O(SeO_3)_2 \rightarrow Mn_2O_3$	713–893	798 endo	74.5	75.0
3. $NH_4Mn(SeO_3)_2 \cdot H_2O$				
$2NH_4Mn(SeO_3)_2 \cdot H_2O \rightarrow 2NH_4Mn(SeO_3)_2$	433–513	393 endo 433 endo	5.7	6.0
$2NH_4Mn(SeO_3)_2 \rightarrow Mn_2(SeO_3)_3$	553–653	533 endo	28.8	26.5
$Mn_2(SeO_3)_3 \rightarrow Mn_2O(SeO_3)_2$	673–773	673 endo	44.8	43.0
$Mn_2O(SeO_3)_2 \rightarrow Mn_2O_3$	793–893	823 endo	77.01	76.2
4. $KMn(SeO_3)_2 \cdot 1.5H_2O$				
$2KMn(SeO_3)_2 \cdot 1.5H_2O \rightarrow 2KMn(SeO_3)_2 \cdot H_2O$	333–352	350 endo	2.4	4.5
$2KMn(SeO_3)_2 \cdot H_2O \rightarrow 2KMn(SeO_3)_2$	493–533	500 endo 540 endo	7.2 21.9	7.5 20.0
$2KMn(SeO_3)_2 \rightarrow K_2SeO_3 + Mn_2O(SeO_3)_2$	633–733	613 exo		
$K_2SeO_3 + Mn_2O(SeO_3)_2 \rightarrow K_2SeO_3 + Mn_2O_2 \cdot (SeO_3)$	753–913	743 endo	36.7	38.5
$K_2SeO_3 + Mn_2O_2(SeO_3) \rightarrow Mn_2O_3 + K_2SeO_3$	913–1113	853 endo	50.26	48.0

compound 1, and cesium diselenitomanganese(III) trihydrate, $CsMn(SeO_3)_2 \cdot 3H_2O$, compound 2, are given in Table 4. Both compounds lose water of crystallization, half mol from compound 1 and 1 mol from compound 2, in the temperature range 323–423 K. The loss upto about 573 K corresponds to the endothermic elimination of 1 and 2 mol of coordinated water from compound 1 and 2, respectively. The thermal decomposition of the anhydrous rubidium compound is complex. Several reactions occur in the range 633–903 K. The mass change upto 803 K corresponds to the loss of 1 mol of selenium dioxide and the formation of Rb_2SeO_3 and manganese(III) oxyselenite. The latter finally appears to decompose to Mn_2O_3 via manganese(III) dioxyselenite. The anhydrous cesium compound decomposes similarly, Table 4. In both these compounds, the observed mass losses at higher temperature are more than the theoretically expected values. This is due to slow decomposition of Rb_2SeO_3 and Cs_2SeO_3 as reported earlier [149,150]. Compound 1 shows a higher temperature range for the formation of oxy- and dioxyselenites, compared with those of potassium [167] and cesium complex selenites.

3.6.5. Thermal behaviour of iron selenites

Giester [78,79] has given a summary of a large number of oxysalts incorporating Fe(III) and Se(IV). $Fe_2(SeO_3)_3 \cdot 3H_2O$ on heating [77] to 873 K in N_2 loses water, Fig. 8, at 413 K ($\sim 1H_2O$) and at 503 K ($\sim 2H_2O$) and then SeO_2 at 643, 668 and 733 K (each step about $1SeO_2$). The total observed mass loss is 71.0 mass % (calculated 70.8 mass %).

Dehydration of $Fe_2(SeO_3)_3 \cdot 5H_2O$ [170] proceeds at 473 K. The amorphous $Fe_2(SeO_3)_3$ crystallizes at 751 K and decomposes to $Fe_2O_3 \cdot 2SeO_2$ at 807 K and to $4Fe_2O_3 \cdot SeO_2$ at 881 K and to Fe_2O_3 at 922 K.

$Fe_2O_3 \cdot 4SeO_2 \cdot H_2O$ decomposes at 681 K to give [81] $Fe_2O_3 \cdot 3SeO_2$, SeO_2 and H_2O, and at 833 K and 893 K to give $Fe_2O_3 \cdot 2SeO_2$ and Fe_2O_3, respec-

Table 4
Thermoanalytical results of Mn(III) selenito complexes [168]

Dehydration/decomposition transition	Temperature (K)		Loss(%)	
	TG	DTA	Calculated	Observed
$RbMn(SeO_3)_2 \cdot 1.5H_2O$				
$2RbMn(SeO_3)_2 \cdot 1.5H_2O \rightarrow 2RbMn(SeO_3)_2H_2O$	323–423		2.1	2.0
$2RbMn(SeO_3)_3H_2O \rightarrow 2RbMn(SeO_3)_2$	423–573	529 endo 600 exo	6.4	6.0
$2RbMn(SeO_3)_2 \rightarrow Rb_2SeO_3 + Mn_2O(SeO_3)_2$	633–903 810 endo 820 endo	670 endo	19.0	20.0
$Rb_2SeO_3 + Mn_2O(SeO_3)_2 \rightarrow Rb_2SeO_3 + Mn_2O_2(SeO_3)$	913–1183	910 endo	30.6	31.0
$Rb_2SeO_3 + Mn_2O_2(SeO_3) \rightarrow Rb_2SeO_3 + Mn_2O_3$	1093–1193	1150 endo	42.6	51.0
$CsMn(SeO_3)_2 \cdot 3H_2O$				
$2CsMn(SeO_3)_2 \cdot 3H_2O \rightarrow 2CsMn(SeO_3)_2 \cdot 2H_2O$	323–433	354 endo 407 endo	3.62	5.2
$2CsMn(SeO_3)_2 \cdot 2H_2O \rightarrow 2CsMn(SeO_3)_2$	433–593	493 endo 603 endo	10.86	11.5
$2CsMn(SeO_3)_2 \rightarrow Cs_2SeO_3 + Mn_2O(SeO_3)_2$	633–743	673 endo	22.07	25.0
$Cs_2SeO_3 + Mn_2O(SeO_3)_2 \rightarrow Cs_2SeO_3 + Mn_2O_2(SeO_3)$	773–873	887 endo	33.26	36.0
$Cs_2SeO_3 + Mn_2O_2(SeO_3) \rightarrow Cs_2SeO_3 + Mn_2O_3$	873–1053	943 endo 1009 endo 1018 endo	44.45	50.0

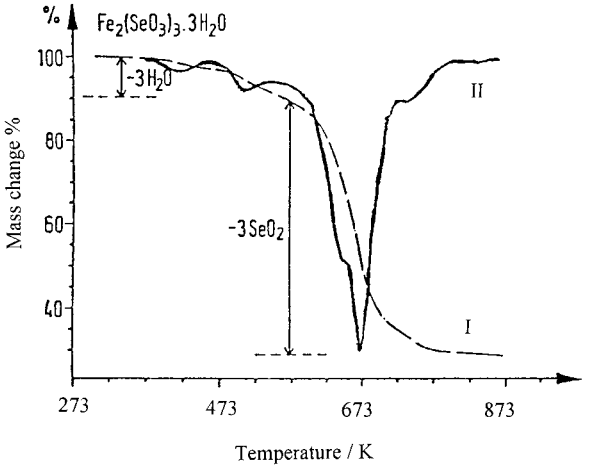

Fig. 8. Thermogravimetry of $Fe_2(SeO_3)_3 \cdot 3H_2O$, heating rate 0.5 K min^{-1}. Decomposition in correlation with temperature, Curve I, and first derivative of this curve, curve II. Adapted from [77].

tively. The IR spectrum of the original reactant is discussed. The absence of an absorption maximum at 1500 to 700 cm^{-1} reveals that H_2O is chemically bound and not H_2O of crystallization.

The TG curve of (fine-grained) crystals of $ZnFe_2(SeO_3)_4$ [85] heated in N_2 upto 1073 K at a heating rate of 20 K min^{-1} shows that decomposition takes place in one step, starting at about 663 K with a maximum at 723 K. The total mass change of 64.7% reflects the release of $4SeO_2$ (calculated 64.8%). The final crystalline decomposition products were identified by X-ray powder diffraction to consist of franklinite, $ZnFe_2O_4$, and minor amounts of zincite, ZnO.

3.6.6. Thermal behaviour of cobalt selenites

There is little information on the thermal dissociation of cobalt selenite dihydrate, $CoSeO_3 \cdot 2H_2O$ [171,172]. Pechkovskii et al. [173] studied the thermal decomposition and the effect of the state of water in the lattice on the thermal dehydration of the solid. Endothermic effects in the DTA curve with minima at 478, 543, and 583 to 633 K are due to the dehydration. The exothermic effect at 733 K corresponds to the crystallization of the amorphous dehydration products and the endotherm at 1033 K to the dissociation of anhydrous cobalt selenite. The XRD pattern of the crystalline dehydration product corresponds to anhydrous $CoSeO_3$ [171]. The XRD of the dehydration product did not show the presence of CoO, but a weak

exotherm at 703 K was assigned to the crystallization of CoO [174]. The final loss of mass in air corresponds to the formation of Co_3O_4, but in vacuum and in argon to CoO [173]. The low temperature decomposition of the selenite anion is associated with the strongly distorted water molecules, in the field of the cation and anion. An analysis of the IR absorption spectra of $CoSeO_3 \cdot 2H_2O$ and its deuterated analogue showed that the water molecules in $CoSeO_3 \cdot 2H_2O$ are not structurally equivalent [173]. The hydrolysis of cobalt selenite with liquid water or its vapour does not occur even under hydrothermal conditions.

Cobalt diselenite, $CoSe_2O_5$, decomposes [101] by losing SeO_2 at about 773 K (observed mass loss = 38%, calculated = 38%) to give $CoSeO_3$, which loses further SeO_2 at 898 K (observed loss = 74%, calculated = 75%) forming CoO as the final decomposition product. The intermediate was amorphous to X-rays. Similar decomposition behaviour was observed for manganese(II) diselenite, $MnSe_2O_5$ [175,176].

Potassium triselenitocobalt(II) dihydrate, $K_2[Co_2(SeO_3)_3] \cdot 2H_2O$, on heating in N_2 in the temperature range 303 to 673 K lost 5.76 mass % between 453 and 543 K with a maximum decrease at 573 K which can be correlated [91] with the loss of approximately two water molecules (calculated 5.88%). The dehydration appeared to be irreversible in analogy with the isotypic compound $Na_2[Zn_2(TeO_3)] \cdot YH_2O$ [177].

3.6.7. Thermal behaviour of nickel selenites

The thermal dehydrations of hydrates of nickel selenite and some properties of the dehydration products and the possible mechanisms of the formation and stabilisation of the disordered phases have been studied [178]. Nickel selenite dihydrate, $NiSeO_3 \cdot 2H_2O$, dehydrates [179,180] in the range 473–673 K, the amorphous dehydration product crystallises at 813 K and the anhydrous salt dissociates at 913–983 K, with the formation of nickel oxide and selenium dioxide [181]. The heat of crystallisation, found from the difference in the heats of formation of the crystalline and amorphous products is 29.924 kJ mol^{-1} [182]. The results of the thermal analysis, together with X-ray diffraction, IR and PMR data, reveal [178] that the complete dehydration of $NiSeO_3 \cdot 2H_2O$ involves two fundamentally different stages. Most of the water is removed in a comparatively narrow temperature range, 423–523 K in air (rate of heating 6 K min^{-1}). The remaining water is removed between 523 and 823 K, almost independently of the pressure. The excess loss in mass, relative to the stoichiometric removal of water, is due to partial decomposition of selenite with the removal of SeO_2 into the gaseous phase, observed throughout the entire dehydration range. The exothermic effect coinciding with complete dehydration and crystallization takes place at 963 K.

Judging from the structure of the isostructural zinc selenite dihydrate, both water molecules in $NiSeO_3 \cdot 2H_2O$ [183] are coordinated to the nickel ion. By analogy with other similar compounds, it may be assumed that the M–O distance in the polyhedron is close to that in NiO, i.e, the coordination polyhedron is fairly rigid. The SeO_4^{2-} ion is a powerful proton acceptor, so strong hydrogen bonds involving the coordinated water molecules are expected.

The dehydration of nickel selenite monohydrate, $NiSeO_3 \cdot H_2O$, is independent of pressure and takes place at 723 K. Spectroscopic data indicate that the water in this hydrate is present in molecular form and is coordinated to the metal. The products of the dehydration of the monohydrate are crystalline, and the loss in mass corresponds to the stoichiometric removal of water [178].

The search for new transition metal oxides with unusual physical and chemical properties has produced [100] another hydrated nickel selenite, $Ni_3(SeO_3)_3 \cdot H_2O$ (or $NiSeO_3 \cdot (1/3)H_2O$), which has been characterized by X-ray single crystal diffraction and thermogravimetric measurements. The TG data, collected in air at 10 K min^{-1}, show [100] that $Ni_3(SeO_3)_3 \cdot H_2O$ loses water and SeO_2, without any discernable intermediates, over the broad temperature range 723–898 K, (observed mass loss = 68%, calculated = 68.00%) to result in a final product of NiO.

3.6.8. Thermal behaviour of copper selenite dihydrate, $CuSeO_3 \cdot 2H_2O$

The thermal dissociation of $CuSeO_3 \cdot 2H_2O$ at various gas pressures was studied [184] by TG, DTA and X-ray analysis. Dehydration occurs in two stages. In the first stage, 2/3 mol of H_2O is lost and the crystalline hydrate $CuSeO_3 \cdot 1(1/3)H_2O$ is formed. Complete

dehydration is accompanied by the decomposition of $CuSeO_3$ and its product is not stoichiometric, but contains upto 80% excess CuO. In addition to the process of crystallization, an exothermic process occurs. Stoichiometric $CuSeO_3$ was prepared [184] and in its thermal dissociation the intermediate $4CuO{\cdot}3SeO_2$ is formed, in addition to $2CuO{\cdot}SeO_2$. No intermediate phase is observed in the decomposition of $CuSeO_3$ under isothermal conditions and under high vacuum. In this case dissociation evidently occurs in one stage with the formation of CuO [184].

3.6.9. Thermal behaviour of silver selenite, Ag_2SeO_3

Berzelius showed that silver selenite melts at a temperature close to the melting point of silver chloride and decomposes at red heat into silver, selenium dioxide vapor and oxygen [185]. The melting point of silver selenite has been found to be 803 ± 5 K. The decomposition of silver selenite below its melting point is very slow. Above its melting point it decomposes

$$Ag_2SeO_3 \rightarrow 2Ag(s) + SeO2(g) + \tfrac{1}{2}O_2(g)$$

3.7. Thermal behaviour of lanthanide selenites

The formation, composition and thermal properties of Y, Nd, Pr, Sm and Gd selenites have been studied [186]. $YSeO_3{\cdot}SeO_3H{\cdot}2H_2O$ and $NdSeO_3{\cdot}SeO_3H{\cdot}(1.5–2)H_2O$ precipitate in the form of elongated rectangular crystals. An attempt to prepare the intermediate Y selenite was not successful. Thermal decomposition of the acidic selenite is discussed. The intermediate Nd selenite can be prepared only by interacting stoichiometric amounts of Nd_2O_3 and SeO_2. The composition of the precipitate in this case corresponds to $Nd_2(SeO_3)_3{\cdot}2H_2O$, while in slight excess of H_2SeO_3 the intermediate selenite is partially transformed into the acidic salt. The IR absorption spectra were taken for some of the compounds.

$M_2SeO_3{\cdot}xH_2O$ compounds, where M = La, Ce, Pr or Nd, are obtained by precipitation from weakly acidic chloride solutions with 20% Na_2SeO_3. Compounds with M = La or Pr begin to lose H_2O of crystallisation at 373 K and are fully dehydrated at 633 and 513 K, respectively, without formation of stable crystal hydrates. The dehydration of compounds with M = Ce or Nd begins at 333 and 353 K, respectively, and continues through the formation of crystal tetrahydrates, stable at 473–573 K for Ce, and 503–843 K for Nd [187].

The thermal stability of selenites of Ce(III) and Ce(IV) has been studied [188]. Thermoanalytical, chemical and X-ray examination indicates that at 433 K $Ce(SeO_3)_2{\cdot}2H_2O$ is dehydrated, and at 873 K loses SeO_2 with the formation of CeO_2. No intermediates were established. Thermal decomposition of Ce(III) selenite is more complex with the formation of intermediates. The final product is CeO_2. DTA and X-ray data indicate [189] that the normal selenites of Ce and Sc are amorphous and undergo crystallization at 693–783 K. On further heating, they completely decompose to CeO_2 and Sc_2O_3.

The amorphous compounds $Ln_2(SeO_3)_3$, Ln = La, Sm, Gd or Y, become crystalline at 728–753 K, and decompose initially to form compounds, $Ln_2O_3{\cdot}(0.9–1.1)SeO_2$ at 1063 to 1173 K. They only form Ln_2O_3 after prolonged heating at above 1473 K. The compounds $Pr_2(SeO_3)_3$ and $Nd_2(SeO_3)_3$ crystallize at 753–763 K, decompose to $Ln_2O_3{\cdot}(1.95–2.05)SeO_2$ (Ln = Pr, Nd) at 1088 K and to $Ln_2O_3{\cdot}(0.0–1.0)SeO_2$ at 1193–1243 K. The compounds $NaY(SeO_3)_2{\cdot}3H_2O$ (I), $Ce_3H(SeO_3)_5{\cdot}5H_2O$ (II) and $M_2(SeO_3)_3{\cdot}4H_2O$ (III) (M = Tb, Dy, Ho, Pr, Tm or Yb) are completely dehydrated [57] at 473 K, no intermediate hydrates are evident from the TG curves. Except for Y and Ce, the anhydrous selenites gradually lose mass beyond 773 K. The anhydrous Y selenite begins to lose mass at 673 K. The anhydrous Ce selenite loses mass with stabilization at 773 K. The anhydrous forms of (III) exhibit endothermic peaks at 393–428 K and exothermic peaks at 873 K, followed by endothermic peaks at 1023 and 1173 K. The anhydrous form of (I) exhibits only endothermic peaks at 438, 481, 703, 1043 and 1095 K, and the anhydrous form of (II) exhibits endotherms at 383 and 892 K and an exotherm at 798 K. The DTA curve of $La_2(SeO_3)_3{\cdot}H_2SeO_3$ showed [190] an endotherm at 473 ± 10 K corresponding to formation of $La_2(SeO_3)_3{\cdot}SeO_2$(II) and an endothermic effect at 773 ± 10 K. Further effects correspond to the stepwise elimination of SeO_2 from the neutral salt with the formation of basic salts.

Pedro et al. [191] reported the characterization by X-ray powder diffraction and IR spectroscopy of $Pr_2Se_4O_{11}$, $R_2Se_3O_9$ (R = La, Pr and Nd) and

R_2SeO_5 (R = Sm, Eu, Gd, Tb, Dy, Y, Ho, Er, Tm, Yb or Lu) phases, as well as proposing a general mechanism for thermal decomposition of rare-earth selenites, which permits the establishment of a structural relationship between the anhydrous materials. The decomposition processes of the anhydrous rare earth selenites can be formulated as

$$\begin{aligned} &R_2(Se_2O_5)\,(SeO_3)_2 \\ &\quad\vert\ -\tfrac{1}{2}SeO_2 \\ &\tfrac{1}{2}R_4\,(Se_2O_5)\,(SeO_3)_{1.5} \\ &\quad\vert\ -\tfrac{1}{2}SeO_2 \\ &R_2(SeO_3)_3 \\ &\quad\vert\ -2SeO_2 \\ &R_2O_2(SeO_3) \\ &\quad\vert\ -SeO_2 \\ &R_2O_3 \end{aligned}$$

All of these stages may be confirmed by a full spectroscopic study of anhydrous rare-earth selenites together with the resolution, by XRD, of the crystal structures of $Pr_2Se_4O_{11}$ and $Pr_2Se_3O_9$ obtained as single crystals, this work was in progress [191] at the reporting time. Knowledge of the structural framework of these materials is the first step in understanding their physical behaviour, such as their magnetic and optical properties. The anhydrous rare-earth selenites constitute a very attractive system, because they include a very large number of new compounds which can be considered as oxides rather than oxosalts [136]. This system contrasts with other comparable systems, such as R–Sb(III)–O or R–Te(IV)–O which show only one phase along the rare-earth element series, $R_3Sb_5O_{12}$ [192] and $R_2Te_4O_{11}$ [193].

3.8. Thermal behaviour of actinide selenites

3.8.1. Thermal behaviour of uranyl selenite, UO_2SeO_3

UO_2SeO_3 is thermally stable upto 823 K. The TG curve, Fig. 9, shows [138] complete decomposition at 923 K. The observed mass loss (29.76%) (823–943 K) can be explained by

$$6UO_2SeO_3 \rightarrow 2U_3O_8 + 6SeO_2 + O_2$$

The DTA curve shows only one endotherm at 933 K corresponding to decomposition. XRD of the uranyl selenite and the final product obtained after heating to 1073 K are comparable to those reported in the literature [137,194].

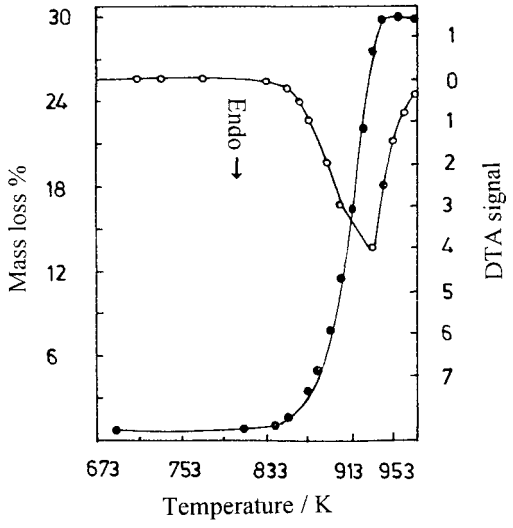

Fig. 9. TG and DTA of UO_2SeO_3. Adapted from [138].

3.8.2. Thermal behaviour of ammonium hexa-aquo triselenito diuranylate, $(NH_4)_2[(UO_2)_2(SeO_3)_3(H_2O)_6]$

The first change that occurs on heating this complex [138] is in the temperature range 433–523 K and the mass loss (Fig. 10) corresponds to the reaction

$$(NH_4)_2[(UO_2)_2(SeO_3)_3(H_2O)_6] \rightarrow UO_2Se_2O_5 + UO_2SeO_3 + 2NH_3 + 7H_2O$$

Between 533 and 633 K

$$UO_2Se_2O_5 + UO_2SeO_3 \rightarrow 2UO_2SeO_3 + SeO_2$$

DTA shows an endotherm at 348–423 K which can be attributed to the partial elimination of water. Another endotherm is observed at 453–653 K. Because the loss of water starts at high temperature, it can be considered that the water molecules are coordinated to the central atom. The IR spectrum of the products, obtained after heating the sample to constant mass at 523 K, shows freedom from NH_4^+ and H_2O. The lines in the XRD of the product of the first stage do not correspond exactly to those of UO_2SeO_3 or $UO_2Se_2O_5$, but suggest a mixture. There are no lines corresponding to free SeO_2, thereby eliminating the possibility of the formation of

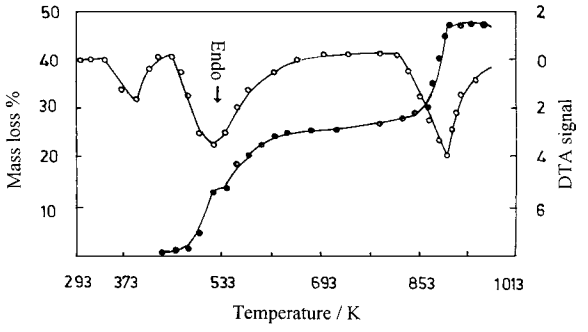

Fig. 10. TG and DTA of $(NH_4)_2(UO_2)_2(SeO_3)_3{\cdot}6H_2O$. Adapted from [138].

$UO_3{\cdot}2SeO_2$ or $UO_2SeO_3{\cdot}SeO_2$. This is in agreement with earlier findings [137,195]. Because the temperature difference between the initiation of the second stage and the completion of the first stage is not appreciable, the DTA shows only one broad endothermic effect (at 513 K) at the heating rate of 9 K min^{-1}.

3.8.3. Thermal behaviour of potassium diaquo triselenito diuranylate, $K_2[(UO_2)_2(SeO_3)_3(H_2O)_2]$

The DTA curve of this complex shows [138] an endothermic peak corresponding to each mass change in the TG. It is rather difficult to identify the species formed at different stages because of the complexity of the system. However, the overall reaction by 1153 K can be represented as

$$K_2[(UO_2)_2(SeO_3)_3(H_2O)_2] \rightarrow K_2U_2O_7 + 3SeO_2 + 2H_2O$$

4. X-ray, IR, Raman and other structural studies on selenites

4.1. Structural studies on uranyl selenites

IR and Raman spectra of uranyl selenite and complex selenites have been examined [138] in the region 4000–250 cm^{-1}. The IR spectrum of uranyl selenite resembles those of alkali metal selenites in the sense that only four vibrations are observed, though there is a marked decrease in ν_3 (Se–O stretching frequency) as compared to that reported [7] and observed in sodium selenite. Coordination via oxygen to the uranyl group should result in lowering of the Se–O stretching frequency compared to the free ion [196]. Coordination via selenium would, on the other hand, raise the frequency. Thus, the observed decrease in ν_3 suggests linking of the selenite ion through oxygen to the uranyl group. This, of course, should result in the lowering of the local SeO_3^{2-} symmetry to Cs and consequently, disappearance of the ν_3 and ν_4 (antisymmetric O–Se–O bending) degeneracy. However, the band ν_3 around 700 cm^{-1} observed in uranyl selenite is somewhat broad and could not be resolved.

The Raman spectra of uranyl selenite and other uranyl selenite complexes, are complicated and show a number of frequencies. Brown [197] has made similar observations on sodium selenite. To interpret these spectra it is necessary to assume that the degeneracy of the antisymmetric modes (ν_3 and ν_4) of the SeO_3^{2-} ion has been removed, due to its site symmetry in the unit cell. The spectrum of uranyl selenite shows a strong band at 829 cm^{-1} which may be the symmetric SeO_3^{2-} stretching mode; while the bands at 731 and 724 cm^{-1} are the split pair of ν_3. A large number of unidentified vibrations are observed [138] in the range 87–237 cm^{-1}.

There is a strong Raman but weak IR band around 800 cm^{-1} in the spectra of all the complexes and it should be due to the ν_1 symmetric stretching frequency of SeO_3^{2-}. The antisymmetric stretching vibration, ν_3, splits with one band appearing at 731 cm^{-1} and the other in the region 814 to 829 cm^{-1} in the Raman spectra. IR spectra show the corresponding bands around 700–730 cm^{-1} and 816–838 cm^{-1}. The large splitting of the degenerate antisymmetric vibration, ν_3 suggests the formation of a bidentate rather than a unidentate complex [198]. The strong band appearing in the region 395–465 cm^{-1} for all selenites can be assigned to the O–Se–O bending (ν_2) mode. The antisymmetric O–Se–O bending (ν_4) is again found to be split, one band appearing in the 390–380 cm^{-1} region and the other around 340 cm^{-1}. An intense IR band corresponding to the antisymmetric vibration, $\nu_3(UO_2^{2+})$ of the uranyl group has been observed at a lower frequency (900 cm^{-1}) in complex selenites, in comparison to uranyl selenite (920–940 cm^{-1}). It may be due to increased ligand contributions to the field of the uranyl ion in complex selenites. The vibration is Raman forbidden for the linear model and does not appear. The non-degenerate

symmetric mode, $\nu_1(UO_2^{2+})$ appears as a strong Raman band doublet at around 878 and 884 cm^{-1}. This would normally be IR forbidden but appears here in all cases as a weak shoulder around 800 to 850 cm^{-1}. However, no Raman shift assignable to $\nu_3(UO_2^{2+})$ is observed either as a high frequency shoulder on ν_1 or as a separate band, indicating the linear configuration of the uranyl group in these compounds.

For the complexes $(NH_4)_2[UO_2)_2(SeO_3)_3(H_2O)_6]$ and $K_2[(UO_2)_2(SeO_3)_3(H_2O)_2]$ the O–H stretching vibrations are observed [138] in the region 3500 to 3300 cm^{-1} and around 1615 cm^{-1} which may be assigned to coordinated water [199,200]. Thermal and IR data of diaquodihydroxo selenito diuranylate, $[(UO_2)_2SeO_3(OH)_2(H_2O)_2]$ reveal the coordination of water and hydroxy groups to the uranyl ions [201]. Large splitting and lowering of the antisymmetric vibrational modes of SeO_3^{2-} suggest the bidentate linkage of the selenite ion through two of its oxygens to the uranyl ion. Negligible solubility in common solvents and high thermal stability indicate its polymeric structure. XRD of all uranyl selenites is complex and shows a number of lines [138].

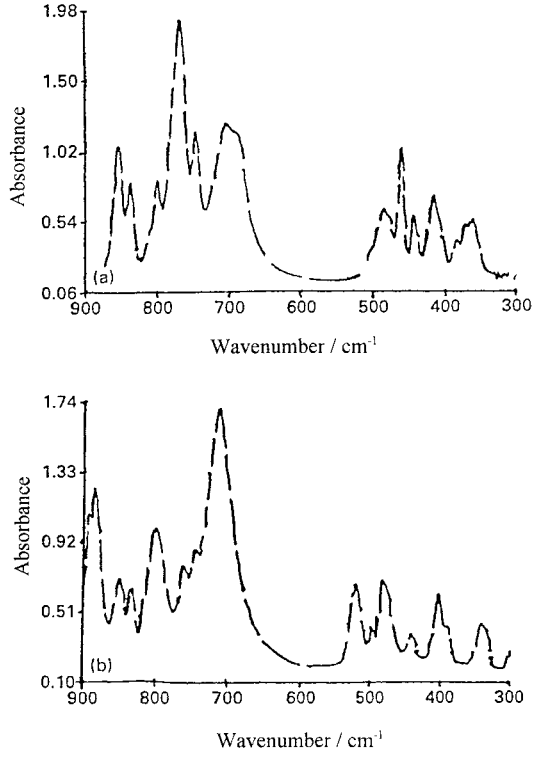

Fig. 11. IR spectra of representative $R_2Se_3O_9$ selenites: (a) $La_2Se_3O_9$ and (b) $Dy_2Se_3O_9$. Adapted from [190].

4.2. Structural studies on lanthanide selenites

The first study [191] of the crystallographic characteristics of rare-earth selenites performed by X-ray single crystal methods for the first group, $R_2Se_4O_{11}$ (R = Y, La, Gd, Tb, Dy, Ho, Er, Tm, Yb, Lu) and by powder methods for the second, $R_2Se_{3.5}O_{10}$ (R = Pr, Nd, Sm, Eu, Gd, Tb) shows that all the reflections can be indexed in the monoclinic system. Crystallographic constants for all $R_2Se_3O_9$ compounds are reported [191]. The values of the unit cell parameters and volumes exhibit the behaviour expected according to the ionic sizes of the different rare-earth cations [202].

R_2SeO_5 compounds give rise to a family of isostructural materials, irrespective of the rare-earth cation size [191]. The most important reflection peaks of the XRD pattern of R_2SeO_5 selenites are related to those of fluorite. Thus, these materials could be described as a super structure of the fluorite type.

Fig. 11 shows the IR spectra of two representative $R_2Se_3O_9$ selenites (R = La, Dy) belonging to different structural types. Both spectra show [191] the characteristic vibrations ν(Se–O) in the region from 895 to 710 cm^{-1}, and those of ν(O–Se–O) between 525 and 355 cm^{-1}, according to a large number of selenites studied previously [7,123].

4.3. Structural studies on transition metal selenites

4.3.1. Structural studies on vanadium selenites

$(NH_4)V_3Se_2O_{12}$ crystallizes in the non-centrosymmetric space group $P6_3$ [9]. The structure can be described as layers of $[V_3Se_2O_2]$ in the *ab* plane of the hexagonal unit cell and cations A (A = K, Rb, Cs in $AV_3Se_2O_{12}$) between the layers. Each layer has vanadium oxide octahedra that share corners to form six-membered rings. The selenite groups cap three corner-sharing vanadium oxide octahedra above and below the layer. The interlayer alkali metal cations are more or less nested inside the vanadium oxide six-membered rings from only one side of the layer. This arrangement of alkali metal with respect to the layer is the only factor that makes the structure non-centrosymmetric [66].

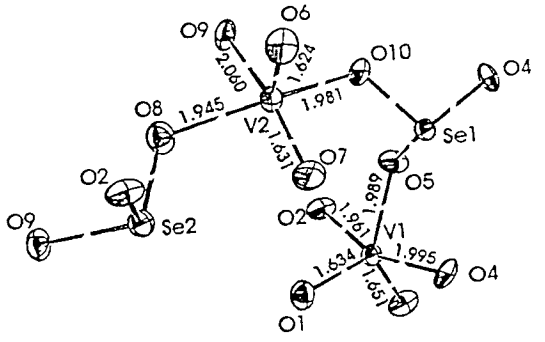

Fig. 12. Asymmetric unit and labeling scheme for $CsVSeO_5$. Important V–O bond distances are shown. Adapted from [66].

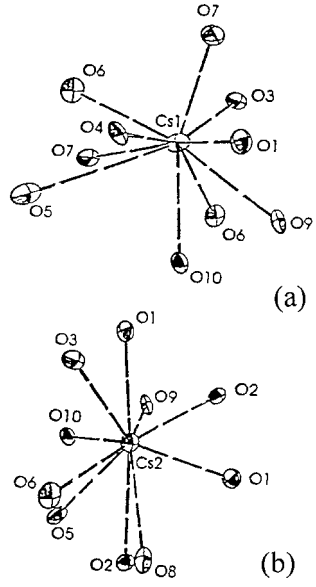

Fig. 13. Oxygens surrounding (a) (top) Cs(1) and (b) (bottom) Cs(2) of $CsVSeO_5$. Adapted from [66].

The structure of $CsVSeO_5$ [66] is completely different from that of $AV_3Se_2O_{12}$. The structure has VO_5 pentahedra and SeO_3^{2-} trigonal pyramids that share corner oxygens to form a three-dimensional network. Cesium atoms fill the empty space of this network. Fig. 12 shows the asymmetric unit and the numbering schemes for the structure. Ideally, five coordinations should have trigonal bipyramid or square pyramid structures or a hybrid of these two [203]. However, the pentahedra found in the present structure deviate from any of these ideal structures. There are two different cesium atoms, Fig. 13. Each of the Cs atoms is surrounded by 10 oxygen atoms with Cs–O distances ranging from 3.028 to 3.75 Å for Cs(1) and from 3.082 to 3.672 Å for Cs(2). The nonbridging oxygens of both VO_5 pentahedra participate in the coordination to Cs atoms more extensively. Of the ten coordinating oxygen atoms, six are vanadyl oxygens for Cs(1) and four are for Cs(2). The $AV_3Se_2O_{12}$ structure appears to be relatively insensitive to cation size, thus, a wide range of cations ranging from K to Cs can be incorporated into this structure. However, Na may be too small to stabilize this structure, rationalizing the inability to synthesize this compound. In contrast, for the $AVSeO_5$ structure, large cations seem to be essential to support the framework and thus, this structure is found only for A = Rb and Cs.

The compounds $AV_3Se_2O_{12}$ (A = NH_4, K, Rb, Cs) are isostructural with $(NH_4)VO_3(SeO_3)_2$ [66]. In $AV_3Se_2O_{12}$ compounds IR peaks observed in the 940–943, 799–825, and 685–692 cm^{-1} ranges were assigned [66] to SeO_3^{2-} symmetric and asymmetric stretching modes of the VO_6 octahedra; respectively. There are a few additional peaks too. The IR spectra for $AVSeO_5$ (A = Rb, Cs) show [66] peaks in the same frequency range as for $AV_3Se_2O_{12}$ and a few more in the 500–574 cm^{-1} range.

The absolute structure of $K(VO_2)_3(SeO_3)_2$ was determined [204] by refining the polarity parameter. Harrison et al. [205] assumed that the asymmetric-synthesized $K(VO_2)_3(SeO_3)_2$ consists of a random 50 : 50 mixture of both enantiomers. However, further measurements are required to establish the relation between each enantiomer and its macroscopic physical properties.

$K(VO_2)_3(SeO_3)_2$ and $NH_4(VO_2)_3(SeO_3)_2$ [9] may be compared with the molybdenum(IV) containing phases $(NH_4)_2(MoO_3)_3SeO_3$ and $Cs_2(MoO_3)_3SeO_3$ [10], which are built up from corner-sharing MoO_6 layers. In these $M_2(MoO_3)_3SeO_3$ phases, the infinite Mo–O layers are capped by Se atoms on one side of the sheet only, as opposed to the Se capping on both sides that occurs in the vanadium-containing materials.

4.3.2. X-ray, IR, Raman and other structural studies on Cr, Mo, and W selenites

Chromium selenite trihydrate, $Cr_2(SeO_3)_3{\cdot}3H_2O$, contains two crystallographically distinct chromium atoms, both octahedrally coordinated, and one distinct

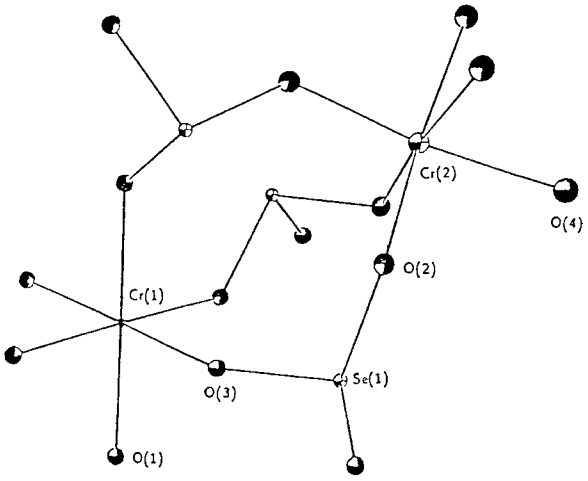

Fig. 14. Structure of $Cr_2(SeO_3)_3{\cdot}3H_2O$, showing Cr–O–Se–O′-Cr′ linkages. Adapted from [35].

3-coordinate selenium site, Fig. 14. Of the four oxygen atoms in the structure, three are involved in Se–O–Cr type linkages, while the remaining oxygen atom, O(4), is in the water molecule and is coordinated only to Cr(2). This structure is isomorphous with those of gallium selenite trihydrate [206] and aluminium selenite trihydrate [33]. There are no direct linkages of octahedra in this structure. The Cr(1) octahedron is typically regular for the $(t_{2g})^3$ central ion, with bond distances varying from 1.976(11) to 2.008(11) Å. Octahedra are linked by Cr(1)–O(1)–Se(1)–O(4)–Cr(1) links, building up an infinite network, Fig. 14.

Single crystal structures and some properties of two new, layered $M_2(MoO_3)_2SeO_3$ compounds ($M = NH_4$, Cs) have been described [10]. These phases are built up from infinite hexagonal tungsten bronze-like, anionic layers of MoO_6 octahedra, capped on one side by pyramidally-coordinated Se atoms. The Mo–O octahedra show an unusual distortion, with displacement of the Mo atom towards an octahedral face, resulting in three short and three long Mo–O bond distances within the MoO_6 unit. Charge compensation is provided by interlayer NH_4^+ or Cs^+ cations.

The hydrothermal syntheses and crystal structures of $M_2(WO_3)_3SeO_3$ ($M = NH_4$, Cs), two new non-centrosymmetric, layered tungsten(VI)-containing phases have been reported [8]. IR, Raman and TG data are also reported [8]. $M_2(WO_3)_3SeO_3$ are isostructural phases built up from anionic layers of vertex-sharing WO_6 octahedra, capped on one side by Se atoms (as selenite groups). Interlayer NH_4^+ or Cs^+ cations provide charge balance. The full H-bonding scheme in $(NH_4)_2(WO_3)_3SeO_3$ has been elucidated [8] from Rietveld refinement against neutron diffraction data. The WO_6 octahedra display three short and three long W–O bond-distances in both these phases. $(NH_4)_2$ $(WO_3)_3SeO_3$ and $Cs_2(WO_3)_3$-SeO_3 are isostructural with their Mo(VI)-containing analogues $(NH_4)_2(MoO_3)_3SeO_3$ and $Cs_2(MoO_3)_3$-SeO_3. $(NH_4)_2(WO_3)_3SeO_3$, Mr = 858.58, hexagonal, space group $P6_3$, $a = 7.2291(2)$ Å, $c = 12.1486(3)$ Å, $V = 549.82(3)$ Å^3, $Z = 2$, $R_p = 1.81\%$ and $R_{wp} = 2.29\%$ (2938 neutron powder data). $Cs_2(WO_3)_3SeO_3$, Mr = 1088.31, hexagonal, space group $P6_3$, $a = 7.2615(2)$ Å, $c = 12.5426(3)$ Å, $V = 572.75(3)$ Å^3, $Z = 2$, $R_p = 4.84\%$ and $R_{wp} = 5.98\%$ (2588 neutron powder data). The Se atom in $(NH_4)_2(WO_3)_3SeO_3$ shows [8] typical pyramidal coordination, Fig. 15, characteristic of the SeO_3^{2-} group [31] and makes three equivalent Se(1)–O(4)–W(1) bonds, each to a different W atom. Of the four distinct oxygen atoms, one, O(2), bonds only to W, two (O(1) and O(3)) bridge pairs of tungsten atoms, and one, O(4) links W and Se.

There are notable similarities in the detailed octahedral-metal coordinations [8]: both tungsten and molybdenum show a distinctive displacement toward

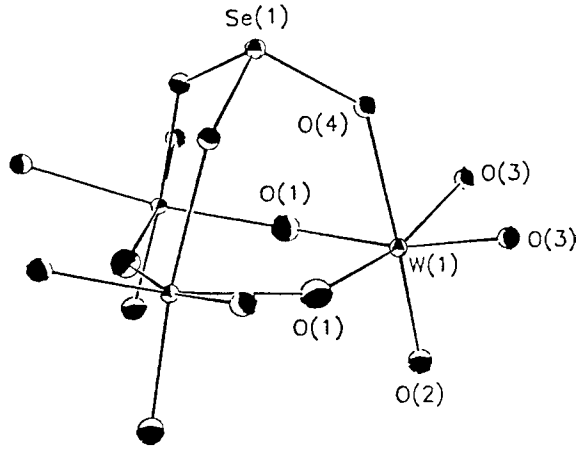

Fig. 15. ORTEP view showing details of the W/Se/O sheet structure in $(NH_4)_2(WO_3)_3SeO_3$, showing WO_6/SeO_3 connectivity via W–O–W and W–O–Se bonds. Adapted from [8].

an octahedral face inside their oxygen atom octahedra, although the magnitude of the Mo atom displacement is somewhat larger than that observed for the W atoms in $(NH_4)_2(WO_3)_3SeO_3$ and $Cs_2(WO_3)_3SeO_3$. The smaller distortion (off centre displacement of W atoms) in the tungsten compounds is consistent with the general observation that distortions around d^0 transition metals increase with increasing cation charge, but decrease with increasing cation size [207].

4.3.3. Structural studies on Mn selenites

The structure of $Mn(II)Mn(III)_2O(SeO_3)_3$ contains [45] three crystallographically different types of MnO_6 octahedra forming $Mn(II)O_4$ chains parallel to (010), and $Mn(III)_2O_7$ net-shaped sheets parallel to (001), which are connected by three types of pyramidal SeO_3 groups, as well as by a common oxygen corner. The $Mn(III)O_6$ octahedra exhibit pronounced Jahn–Teller elongations, whereas a similar distortion of the $Mn(II)O_6$ polyhedron is attributed to interpolyhedral connections. The oxo-oxygen is coordinated to three Mn(III) cations within the Mn_2O_7 sheets with very short Mn–O bond lengths.

Koskenlinna et al. [72,93,175,176] gave a structural description of $MnSe_2O5$ in an orthorhombic system. This variety was found to be isostructural with $ZnSe_2O5$ [40]. J. Bonvoisin et al. [39] determined the crystal structure of the *m*-variety and compared it with the *o*-variety. Both structures present similarities (1) zigzagging chains of octahedra (MnO_6), running along the (001) axis; (2) each octahedron shares opposite edges with the two neighbouring ones; (3) Mn-Mn intrachain distances are similar; (4) each chain is interconnected with six other chains, via $Se_2O_5^{2-}$ anions. Differences between the *m*- and *o*-form are also apparent (1) the zigzagging angle is sharper in the *m* form; (2) the bridge angle Se–O–Se is higher in the *m*-form in comparison to other diselenites, including the *o*-form; (3) interchain distances range from 5.169 to 7.965 Å for *m*, and between 6.190 to 6.822 Å for the *o* form. Differences are also noticed in the IR spectra. The phase transformation $m \leftrightarrow o$ does not occur by heating even upto decomposition. A magnetic study of both varieties shows a weak antiferromagnetic interaction between ions along a chain and reveals the occurrence of a long range antiferromagnetic ordering at significantly different temperatures: $T_N = 9$ and 5.2 K for *m*- and *o*-species, respectively. A magneto structural correlation is proposed.

Relatively small and irregular distortions of the MnO_6 octahedra within the compounds $MnSeO_3 \cdot D_2O$ and $MnSe_3 \cdot 2H_2O$ were described [175,176]. In the divalent manganese ion, d electron density is spherically distributed and does not contribute to the possible distortions of the coordination polyhedra. As a result, the MnO_6 octahedra may be quite regular in some compounds as in $MnSe_2O_5$, where the differences in bond lengths are statistically insignificant [175,176]. In this respect divalent manganese differs greatly from trivalent manganese, which is expected to exhibit distortions of the Jahn–Teller type in octahedral coordination owing to its high-spin d^4 configuration.

Manganese(III) selenite trihydrate, $Mn_2(SeO_3)_3 \cdot 3H_2O$ [72], and manganese(III) hydrogen selenite diselenite, $MnH(SeO_3)(Se_2O_5)$ [93], are monoclinic. Their crystal data have been given [72,93]. In $Mn_2(SeO_3)_3 \cdot 3H_2O$ the three non-equivalent manganese atoms are octahedrally coordinated and the coordination polyhedra exhibit Jahn–Teller distortions. All the octahedra are tetragonally elongated and two of the three non-equivalent octahedra have an additional small axial distortion in the equatorial plane. Each selenite bridges three different MnO_6-octahedra linking them into a three-dimensional network. The bonding scheme of the selenium is pyramidal and the bond lengths and angles are within the normal range [72].

The MnO_6 octahedron is distorted by Jahn–Teller forces, with Mn–O bonds ranging from 1.916 to 2.179 Å in $MnH(SeO_3)(Se_2O_5)$. The compound contains both selenite and diselenite groups which act as bridging ligands between two and three Mn atoms, respectively. The Se–O bonds range between 1662 and 1776 Å in the selenite and between 1.664 and 1.803 Å in the diselenite group [93].

4.3.4. Structural studies on iron selenites

Giester and Pertlik [77] investigated $Fe_2(SeO_3)_3 \cdot 3H_2O$ thermally and determined its structure by single-crystal XRD techniques. Structure determinations on the following Fe(III)–Se(IV) oxosalt compounds have been performed: $FeH(SeO_3)_2$ [208], $Fe_2(SeO_3)_3 \cdot 6H_2O$ [209], $Fe(HSeO_3)(Se_2O_5)$ and $Fe(HSeO_3)_3$ [210], $Fe_2(SeO_3)_3 \cdot H_2O$ [49], KFe-

$(SeO_3)_2$ [86], $LiFe(SeO_3)_2$ [87], $LiFe(Se_2O_5)_2$ [88], and the Se(IV)–Se(VI) compound $Fe(SeO_2OH)(SeO_4)\cdot H_2O$ [211] plus Se(VI) compounds: $Fe_2(SeO_4)_3$ [212], $NaFe(SeO_4)_2$ [213] and $RbFe(SeO_4)_2$ [214].

Investigations have shown [215] 12 forms of iron(III) selenites in the Fe_2O_3–SeO_2–H_2O system. Such an abundance of forms hinders the use of methods such as XRD and IR spectroscopy for the identification and quantitative determination of iron(III) selenites. Hence the investigation of $^{57}Fe^{3+}$ Mössbauer spectra is of interest in this connection. In addition, Mössbauer spectra allow independent information to be obtained about the structural and chemical character of the compounds being studied.

The Mössbauer spectra of iron(III) selenites of the type $Fe_2O_3\cdot xSeO_2\cdot yH_2O$ ($x = 2$, 3, 4 or 6; $y = 0$, 1, 3 or 7) with idealised compositions have been obtained [216] for the first time. The oxide selenite $Fe_2O_3\cdot 2SeO_2$ changes above 77 K (probably at 80 to 100 K) into a magnetically ordered state. Iron(III) has octahedral coordination in all the above selenites, but in the oxide selenite 25% of the Fe^{3+} ions have tetrahedral coordination.

Iron selenite monohydrate, $Fe_2(SeO_3)_3\cdot H_2O$ is monoclinic [49], space group $P21/n$, $a = 7.955(2)$ Å, $b = 9.890(2)$ Å, $c = 11.538(3)$ Å, $b = 101.65(1)^\circ$, $Z = 4$, $R = 0.0042$, $R_w = 0.037$ for 2188 reflections. Atomic coordinates are given. $[Fe1^{(60)}\ Fe2^{[50+10w]}O_{10}]$ groups of edge-sharing Fe(III)-polyhedra are corner connected via $Se(IV)O_3$ pyramids to a framework structure. Octahedral Fe–O distances are 1.954 to 2.102 Å for Fe1 and 1.928 to 2.117 Å for Fe2 with mean bond lengths of 2.007 and 2.015 Å. The selenite groups are moderately distorted, the mean Se–O lengths are 1.681, 1.695 and 1.708 Å. With the exception of O4, O9 and Ow, all oxygen atoms are coordinated to one Fe and one Se atom with Fe–O–Se bond angles ranging from 120.10° to 139.30°.

A valence bond calculation for Ow leads to a value of 0.38 v.u (valence units), definitely proving the presence of a water molecule. Neglecting Ow–O bonds within the Fe2 polyhedron, there are four Ow–O contacts of less than 3.64 Å which come into consideration for H-bonding. Bond lengths, bond valence calculations, and the bond angles Se–O–Fe for these atoms have been given [49].

The $LiFe(Se_2O_5)_2$ structure was investigated [88] by single crystal XRD methods. Hawthorne et al. [217] showed the *Pnca* space group in $Co(Se_2O_5)$ with chains of edge-sharing CoO_6 octahedra running parallel to [100] and sharing corners with Se_2O_5 groups. The atomic arrangement in $LiFe(Se_2O_5)_2$ can be derived from the $Me(Se_2O_5)$ structure type by substitution of half the divalent cobalt atoms by Li, and the other half by ferric iron. This alternating order leads to the acentric space group *Pnc*2. Nevertheless, a refinement in *Pnca* (with a statistical distribution of Li and Fe) gives R values of about 0.08 indicating the close structural relationships [88]. The isostructural compounds $MeSe_2O_5$ (Me = Mn, Co, Zn) have a close structural relation to $LiFe(Se_2O_5)_2$.

$LiFe(SeO_3)_2$ is tetragonal [87] with space group $\overline{1}42d$, $a = 10.649(2)$ Å, $c = 9.959(2)$ Å, $V = 1129.4$ Å^3, $Z = 8$, 1268 unique reflections, $R = 0.037$. The structure contains $LiFeO_8$ groups, built up by FeO_6 octahedra edgesharing with strongly distorted LiO_4 tetrahedra. These $LiFeO_8$ groups share corners with trigonal pyramidal SeO_3 groups to form a three-dimensional network. The mean bond lengths are 1.994, 2.006 and 1.699 Å for Li–O, Fe–O and Se(IV)–O, respectively.

$KFe(SeO_3)_2$ has space group *Pnma* [86], the monovalent cation is 8-coordinated, all polyhedra arranged on the mirror plane, realizing a distinctly different structure type. The FeO_6 octahedra are isolated from each other, corner connecting with SeO_3 pyramids and sharing common edges with the KO_8 polyhedra.

$ZnFe_2(SeO_3)_4$ crystals exhibit monoclinic holohedral symmetry [85] with the forms [010], [100], [011], [111], and [111] visible. Details of the crystal data are reported.

4.3.5. Structural studies on Co and Ni selenites

The crystal structure of a hydrothermally synthesized new modification of $CoSeO_3$, ($CoSeO_3$-II), was determined [89] by direct and Fourier methods using single crystal XRD. It is monoclinic, space group *C*2/*c*, $a = 15.646(3)$ Å, $b = 9.947(2)$ Å, $c = 14.984(3)$ Å, $b = 110.65(1)$ Å, $Z = 32$, $R_w = 0.038$ for 2948 unique reflections.

The structure of $CoSeO_3$-II is closely related to that of $Co_3(SeO_3)_3\cdot H_2O$ [94] and the isotypic compound $Ni_3(SeO_3)_3H_2O$ [97,100]. $Co_3(SeO_3)_3\cdot H_2O$ is built up from $[Co_5(SeO_3)_6\cdot H_2O]$ sheets which contain similar

structural units as found in $CoSeO_3$ [93]. The unusual position of selenite pyramids within the notches between edge-sharing CoO_6 octahedra is topologically identical with the situation in $CoSeO_3$-II and leads to comparable polyhedral distortion. These sheets are tied together by single CoO_6 octahedra, thereby, in analogy with $CoSeO_3$-II, forming a system of intersecting channels, occupied by lone-pair electrons of the Se(IV) atoms [94]. The high pressure modification of $CoSeO_3$, investigated by Kohn et al. [96], forms a completely different structure. In the course of Wildner's investigations of Co^{2+} and Ni^{2+} selenites [95,218], the crystal structures of $NaCo_2(SeO_3)_2(OH)$, $CoSeO_3{\cdot}2H_2O$ and $NiSeO_3{\cdot}2H_2O$ were determined or refined.

Wildner [91] reported the first synthesis and crystal structure of zemannite-type selenites $K_2[M_2(SeO_3)_3]{\cdot}2H_2O$ (M = Co, Ni). The investigations confirmed the zemannite structure type, a framework structure with wide channels running parallel to [001]. The space group was $P6_{3/m}$, $a = 9.091(3)$ Å, 9.016(2) Å, $c = 7.562(2)$, 7.476(2) Å, $Z = 2$, $R_w = 1.6$, 2.5%. In both compounds four maxima were clearly located in the channel by Fourier summations and attributed to two K atoms and two H_2O molecules, each with an occupancy factor of 1/6. A possible ordering scheme (full occupancy) with local symmetry 1- and 6-coordinated K atoms could be derived for the channel atoms.

The structural features of $K_2[M_2(SeO_3)_3]{\cdot}2H_2O$ in respect to the framework are essentially the same as described for zemannite [179,219]. Pairs of face-sharing $M(II)O_2$ octahedra are connected via SeO_3 pyramids forming a honeycomb-like hexagonal $[M(II)_2(SeO_3)_3]^{2-}$ framework with wide channels running parallel to [001]. The basal oxygen planes of the SeO_3 pyramids border the channels, whereas the apical Se atoms are situated inside the walls of the framework. Nevertheless, the lone-pair electrons of each Se(IV) atom extend into its neighbouring channel, consequently, zemannite type compounds can be classified as microporous structures with heteroatomic walls [220].

Leider and Gattow found that $CoSe_2O_5{\cdot}3H_2O$ was isostructural with the Ni and Zn analogues and the same workers [97] reported that $CoSeO_3{\cdot}2H_2O$ adopted the same structure as the Ni, Zn, Mg, Mn and Cu selenite dihydrates. Harrison et al.[101] reported the synthesis and structure of $CoSe_2O_5$, which is once again isomorphous with the M^{2+} analogues $ZnSe_2O_5$ [40] and $MnSe_2O_5$ [175,176]. It contains a discrete $Se_2O_5^{2-}$ unit which was also found by Hawthorn et al. [217]. $CoSe_2O_5$ is orthorhombic with space group *Pnab*, $a = 6.075(2)$ Å, $b = 10.366(2)$ Å, $c = 6.791(8)$ Å, $V = 427.8$ Å^3, $Z = 4$, $Dx = 4.61$ kg m^{-3}. The structure consists of strings of edge sharing CoO_6 octahedra running parallel to edge a, crosslinked by O–Se–O linkages, which may be considered to be part of discrete $Se_2O_5^{2-}$ units.

4.3.6. Structures of zinc selenites

A few zinc selenites have been reported in literature [85]. Table 5 shows their selected details. These ZnO_n ($n = 5, 6$) coordination polyhedra are of low symmetry with bond length and bond angle distortions reflecting the respective interpolyhedral linkage.

In general, Zn^{2+} (a $3d^{10}$ ion) is expected to form Zn–O polyhedra with regular geometry, eventhough its coordination figure may be considerably distorted. Commonly, Zn^{2+} is coordinated to oxygen ligands in tetrahedral, trigonal bipyramidal, tetragonal pyramidal, or octahedral arrangements. Mean Zn–O distances reported [219] are 1.956, 2.052 and 2.112 Å for 4-, 5-, and 6-coordination, respectively. A comparison of $ZnFe_2(SeO_3)_4$ with the crystal structure of $Zn_3Fe_2(SeO_3)_6$ [79] shows that in both compounds complicated frameworks are formed by linkage via corners and edges with quite similar distortions of bond lengths and angles for the FeO_6 octahedra and ZnO_5 groups, respectively. The rather short Zn–Se distances in both compounds are caused by common edges of SeO_3 and ZnO_5 groups. In $Zn_3Fe_2(SeO_3)_6$, some of the zinc atoms have a distorted octahedral environment with a mean Zn(6)–O distance of 2.116 Å, and a different formal 'subunit', a centrosymmetric arrangement of five edge-sharing polyhedra of the type FeO_6–ZnO_5–ZnO_6–ZnO_5–FeO_6 occurs.

4.4. Structural studies on Al, Ga and In selenites

Morris et al. [165] reported syntheses and crystal structures of two novel aluminium selenites, $Al_2(SeO_3)_3{\cdot}6H_2O$ and $AlH(SeO_3)_2{\cdot}2H_2O$. The former is trigonal (space group $P3_{1c}$). The structure consists

Table 5
Data on zinc selenites

	$ZnSe_2O_5$	$ZnSeO_3$	$ZnSeO_3$	$ZnSeO_3 \cdot 2H_2O$	$Zn(HSeO_3)_2 \cdot 2H_2O$	$Zn_3Fe_2(SeO_3)_6$	$Zn_2Fe(SeO_3)_4$
Space group	*Pbcn*	*Pnma*	*Pcab*	*P*21/*n*	*P*21/*c*	*P*21/*c*	*Pc*
Coordination of the Zn atom	[6]	[6]	[5]	[6]	[6]	[6] [5]	[5]
Site symmetry of the Zn atom	2	1	1	1	1	1 1	1
Range of Zn–O distances (AO)	2.099–2.130	2.089–2.223	1.973–2.195	1.97–2.32	2.072–2.126	2.025–2.256 2.013–2.159	2.005–2.133
<Zn–O>	2.113	2.163	2.058	2.107	2.102	2.116 2.069	2.049
Bond length distortion, Å	0.00004	0.00066	0.00184	0.00260	0.00011	0.00225 0.00062	0.00054
Nearest Zn–Se distance, Å	3.20	3.11	3.17	3.21	3.36	3.231 2.912	2.915
Polyhedral linkage of Zn	edge-linked to chains	corner-linked to network	dimers by edge, sheet by corners-	dimers by edge	isolated polyhedra	Fe–Zn "clusters"	Fe–Zn "clusters"
References	[40]	[96]	[a]	[b]	[c]	[79]	[85]

Bond length distortion: $(1/n)\Sigma[(d_i - d_m)/d_m]^2$ $(n = 5,6)$
[a]F.C. Hawthorn, T.S. Ercit and L.A. Groat, Acta Crystallogr. C42 (1986) 1285.
[b]V.F. Gladkova, Y.D. Kondrashev, Sov. Phys. Cryst. 9 (1964) 149.
[c]Y.D. Kondrashev, Y.Z. Nozik, L.E. Fykin and T.A. Shabinova, Sov. Phys. Cryst. 24 (1979) 336.

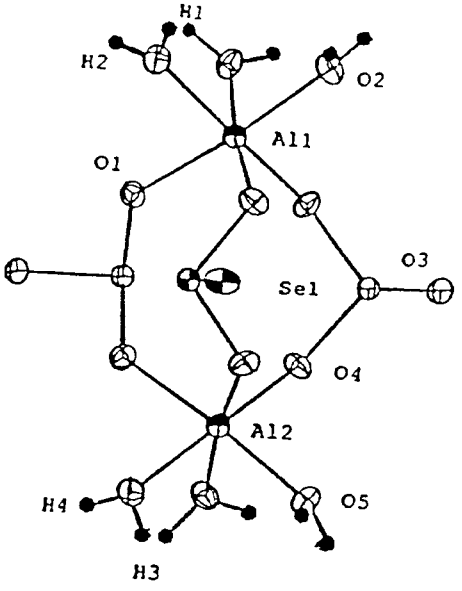

Fig. 16. The molecular unit present in $Al_2(SeO_3)_3{\cdot}6H_2O$. Adapted from [165].

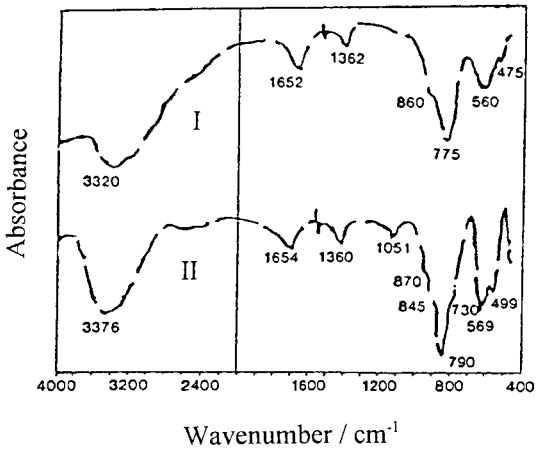

Fig. 17. IR spectra of $Al_2(SeO_3)_3{\cdot}6H_2O$ (I) and $AlH(SeO_3)_2{\cdot}2H_2O$ (II). Adapted from [165].

of discrete $Al_2(SeO_3)_3{\cdot}6H_2O$ units which are linked via H-bonding to form an open structure with channels running parallel to the [0001] direction. $AlH(SeO_3)_2{\cdot}2H_2O$ is monoclinic ($P21/n$). The structure consists of octahedral AlO_6 units which are interlinked via the sharing of vertices with four separate selenite groups. The selenite groups form dimers which appear to contain a symmetry-restricted H-bond. This symmetry-restricted bond is markedly shorter than the other H-bonds in the structure. The molecular unit present in $Al_2(SeO_3)_3{\cdot}6H_2O$ is shown in Fig. 16. The structure contains almost regular octahedral aluminium (average Al(1)–O distance =1.898(4) Å, average Al(2)–O distance = 1.899(4) Å, O–Al–O angles ranging from 84.1(1)° to 93.1(2)° and trigonal pyramidal SeO_3 groups. Crystal data, final atomic coordinates, thermal parameters, bond distances and angles are given [165].

The H atom in $AlH(SeO_3)_2{\cdot}2H_2O$ could not be found by difference Fourier methods, but analysis of the IR spectrum, Fig. 17, reveals no evidence for two distinct types of selenite group. Such a result indicates [165] that the final proton is shared between two selenite groups to form a (SeO_3HSeO_3) dimer.

Other selenites of group 13 metals, that have been characterized by single crystal diffraction methods include $Ga_2(SeO_3)_2{\cdot}3H_2O$ [206], which is isostructural with the corresponding aluminium compound [33], and $CsGa_2H(SeO_3)_4{\cdot}2H_2O$ [221]. A number of other compounds have been tentatively characterized by means of their IR spectra [222]. The IR spectrum of $Ga(HSeO_3)(Se_2O_5){\cdot}1.075\ H_2O$ shows a complicated band structure in the selenite ion stretching region due to the presence two types of ion, diselenite and hydrogen selenite [11]. The Se–O–Se δ band is seen at 990 cm^{-1}. The low energy (400–600 cm^{-1}) region shows a number of bands that cannot be unambiguously assigned. Other assignments were made by comparison with other spectra of selenite species [38,175,176].

4.5. Structural studies on divalent metal selenites

Weiss [223] elucidated the crystal structure of $MgSeO_3{\cdot}6H_2O$. IR spectra, XRD patterns of $MSeO_3{\cdot}xH_2O$, $M(HSeO_3)_2{\cdot}xH_2O$, MSe_2O_5 (M = Mg, Ca, Sr, Ba, Zn and $x = 0$–6) and their deuterated derivatives have been reported [18,23,24,116]. The force constants of the Se–O bonds for these selenites were calculated from the IR spectra, Table 6. It follows that the force constants in the SeO_2 groups in the hydrogen selenite and diselenite anions are somewhat higher than in the SeO_3^{2-} group, Table 6. On the other hand, the force constants in the SeOH and Se–O–Se groups are much lower than for the SeO_3^{2-} group. The situation is analogous for alkali metal selenites and

Table 6
Force constants for the selenium-oxygen bonds

S.No	Substance	Group	ν_s (cm^{-1})	ν_{as} (cm^{-1})	KSeO (Nm^{-1})	Ref.
1	$MgSeO_3 \cdot 6H_2O$	SeO_3	714	835	498	
2	$Mg(HSeO_3)_2 \cdot 4H_2O$	SeO_2	865	780	532	
		SeOH	652	–	333	[23]
3	$MgSe_2O_5$	SeO_2	870	790	541	
		Se–O–Se	577	–	266	
4	$CaSeO_3 \cdot H_2O$	SeO_3	731	815	487	
		SeO_2	853	787	487	
5	$Ca(HSeO_3)_2 \cdot H_2O$	SeOH	656	–	337	
6	$CaSeO_3$ anhydrous crystal I	SeO_3	734	816	485	
		SeO_2	881	820	567	[18]
7	$CaSe_2O_5$	Se–O–Se	540	–	229	
8	$Ca_2Se_3O_8$	Se–O–Se	593	–	276	
9	$SrSeO_3 \cdot nH_2O$	SeO_3			496	
10	$SrSeO_3$ anhydrous crystal I	SeO_3			495	
11	$Sr(HSeO_3)_2$	SeO_2			535	
		SeOH			308	
12	$SrSe_2O_5$	SeO_2			565	[24]
		Se–O–Se			268	
13	$BaSeO_3$	SeO_3			491	
14	$BaSe_2O_5$	SeO_2			540	
	Se-O-Se				241	
15	$ZnSeO_3$	SeO_3			464	
16	$Zn(HSeO_3)_2 \cdot 2H_2O$	SeO_2			480	
		SeOH			350	[116]
17	$ZnSe_2O_5$	SeO_2			526	
		Se–O–Se			241	

zinc selenites [116]. The force constants of Se–O bonds in $MSeO_3$ selenites and their hydrates lie in the range of 485 to 498 Nm^{-1}, Table 6. No substantial differences in the bond force constants were observed between the hydrates and the anhydrous salts. The Se–O bond force constants in the SeO_2 groups lie in the range of 528 to 535 Nm^{-1} and 548 to 567 Nm^{-1} for hydrogen selenites and diselenites, respectively. The Se–O bond force constant in the SeOH groups of hydrogen selenites falls in the range of 308 to 337 Nm^{-1}, while those of the Se–Se bonds in diselenites are between 229 and 268 Nm^{-1}.

Comparison of the values of the force constant in the SeOH group in the series of divalent metal hydrogen selenites shows that the Se–O bond is strongest in zinc hydrogen selenite dihydrate [115]. Consequently, the O–H group here is weakest, and so it is broken down most readily to give the diselenite, Se–O–Se, group and release water. The bonding properties also reflect in the substantially lower decomposition temperature of $Zn(HSeO_3)_2 \cdot 2H_2O$ giving $ZnSe_2O_5$ and releasing water, as compared with the analogous $Co(HSeO_3)_2 \cdot 2H_2O$ and $Ni(HSeO_3)_2 \cdot 2H_2O$. While the zinc salt decomposes at 283 to 363 K, the cobalt and nickel salts, possessing considerably lower KSeO values in the SeOH groups, decompose at temperatures as high as 353 to 473 K. Similarly the strength of the Se–O bond decreases in acid cadmium(II) and mercury(II) selenites in comparison with acid zinc selenite [116]. The spectra were also evaluated to obtain hydrogen bond energies and lengths from the positions of the hydroxyl group stretching vibration bands [7,18,115,224]. Assuming that no interbond tunnel effect is present in the compounds $Cd_3H_2(SeO_3)_4$ and $Hg_3H_2(SeO_3)_4$, hydrogen bond lengths were found to lie in the ranges 2.55 to 2.60 Å and 264 to 269 Å for Cd(II), and Hg(II) salts, respectively. These are all bonds of the anion–anion type that the observed lengths indicate hydrogen bonding to be between strong and medium strong. The lengths determined for the hydrogen bonds are comparable with hydrogen bonds in other known

selenites of divalent metals [18,23,24,115,126,225]. Two water-to-anion hydrogen bonds with lengths 2.793 ± 0.005 and 2.661 ± 0.004 Å and anion–anion bond length 2.657 ± 0.0005 Å are present in $Zn(HSeO_3)_2 \cdot 2H_2O$ [225]. These values classify the hydrogen bond in question between weak and medium [115].

For the anhydrous selenites in the Mg through Ba series prepared by thermal decomposition of the selenite hydrates and diselenites and, in the case of calcium [18] also the triselenite, polymorphism is observed. In view of the marked similarity of the powder XRD patterns of some of the anhydrous selenites, the substances can be considered to be of similar structure. Especially pronounced is the similarity between the high temperature modification of $SrSeO_3$ and $BaSeO_3$. In addition to the temperature and method of preparation, the formation of the various modifications is, obviously, governed by the polarizing ability of the cation [24].

4.6. Structural studies on alkali metal selenites

Paetzold [19,20] systematically measured the IR spectra of the selenites and from the spectra of alkali metal selenites, determined the approximate constitution and symmetry of selenite, hydrogen selenite, and the selenium oxygen bonds.

Heat treatment of Rb_2SeO_3 at temperatures upto 473 K entails an insignificant mass loss. The diffraction trace becomes slightly simpler, the IR spectra remain almost the same as that of the initial salt. The product remains hygroscopic and the intense δ(Se–OH) band at 1338 cm^{-1}, which appears in the spectra of all hygroscopic alkali metal selenites following their hydration, indicates the presence of a hydrolysed form of the selenite [149]. The inflections at 840 and 880 cm^{-1} which are absent from the spectrum of the products obtained at 473 K are, probably, caused both by the appearance of selenate ions above 583 K and the presence of acid selenites formed as a result of hydrolysis. There are intense high wavenumber bands in the spectra of the products obtained at 873 K [149], in the range of ν(Se–O) 875 and 900 cm^{-1}, which are characteristic of SeO_4^{2-}. Their intensity increases with increase of the temperature at which the product is formed (from 673 K upwards). The bands due to the deformation vibrations of selenite ions (430 cm^{-1}) are also displaced towards lower wavenumbers (to about 412 cm^{-1}) which is likewise characteristic of selenates [226]. Above 973 K the composition of the oxidation products is stabilised and corresponds to the formula $Rb_2SeO_3 \cdot 3Rb_2SeO_4$. The ν(Se–O) bands in the region of about 875 cm^{-1}, characterising selenate ion, are the most intense in the IR spectra of the products $Rb_2SeO_3 \cdot 3RbSeO_4$ obtained at 1123 or 1323 K. The diffractometer traces of the $Rb_2SeO_3 \cdot 3Rb_2SeO_4$ specimens differ appreciably from those of the products obtained at lower temperatures. It is noteworthy that, in certain spectra, the deformation vibrations of the O–H bonds in the admixtures of hydrolysed selenite species are displaced towards higher values compared with the spectra in liquid paraffin [149]. Thus, spectra of moisture containing specimens in liquid paraffin show bands in the region of 1300–1340 cm^{-1}, while in the spectra of the specimens in KBr, they are displaced to about 1415 cm^{-1}, the wavenumbers in the region of ν(Se–O) remaining unchanged.

A similar band shift has been observed in the spectra of the heat treatment products of potassium and cesium selenites [227], particularly those obtained at low temperatures. The ratios of the ν(SeO) band intensities of the selenite and selenate ions in the spectra of the Rb_2SeO_3 heat treatment products in liquid paraffin and KBr are slightly different.

Comparison of the result of the X-ray diffraction analysis of potassium [228], rubiduim [229] and cesium [230] selenites and also their heat treatment products shows [152,227] that the rubidium compounds give rise to the simplest diffractometer traces. Comparison of the IR spectra of the same substances also reveals [151,227,231] a greater simplicity of the spectra of the rubidium salts. Possibly, the explanation is the relatively lower hygroscopicity of the rubidium compounds (compared with the potassium and cesium salts) and hence a smaller amount of the hydrolysed species derived from selenite ions, present as an admixture in the rubidium compunds [149].

IR spectra of ammonium selenite indicate a decrease in the assumed C_{3v} symmetry of the anions [153]. The spectrum of ammonium hydrogen selenite corresponds to Cs anion symmetry and is characterised by a typical intense band of the stretching vibration of the Se(OH) group at $\nu = 613$ cm^{-1} and a relatively strong band for the bending vibration of

the OH(Se) group at $\nu = 1160\ cm^{-1}$. It follows from analysis of the spectrum of the other acid salt, ammonium trihydrogen bis(selenite), that this compound contains $HSeO_3^-$ groups, while the H_2SeO_3 group could not be found. A spectrum with similar character was observed [146] for the compounds of the $MH_3(SeO_3)_2$ type (M = K, Rb or Cs). The structures of which are characterized by location of two protons in ordered positions. The third proton occupies a disordered position and the vibration corresponding to the H_2SeO_3 group does not appear in the spectrum [153].

In the study of the IR spectra of acid lithium, thallium(I) [232] and potassium [14] selenites attention has mainly been directed toward clarification of the behaviour of protons from the viewpoint of their ordering, as they decisively effect the dielectric properties of the substances [233–236]. The spectrum of lithium hydrogen selenite is marked by characteristic intense bands of the stretching vibration of the SeO(H) group and bending vibration of the OH(Se) group, corresponding to a hydrogen bond length of 2.616 Å, found in the X-ray study [237]. The protons in this hydrogen bond are thus located symmetrically in the ordered position, i.e., at the lowest discrete levels of the two minimum asymmetrical potential function, with a virtually zero probability of tunnelling [234]. In the spectra of $LiH_3(SeO_3)_2$ and $TlH_3(SeO_3)_2$ absorption bands were found in the region of normal anion vibrations that suggest the presence of the $HSeO_3$ and H_2SeO_3 groups in the structure. Hence, at least two protons in these compounds are located in the hydrogen bond analogous to $LiHSeO_3$, i.e., asymmetrically in ordered positions. This conclusion has also been verified for $LiH_3(SeO_3)_2$ by a study of the structure [238–241] and is manifested by the ferroelectric behaviour of the substance in the whole temperature of existence region.

The absorption bands for $K_5H_3(SeO_3)_4$ demonstrated [14] the presence of hydrogen selenite ions $\delta_s(SeO_2)XSeO_3$ (X = H or D) 435 s, $\nu_{as}(SeO_2)(HSeO_3^-)$ and $\nu_s(SeO_2)(HSeO_3^-)$ 824 s. Thus, as in $KHSeO_3$, protons occupy the ordered positions in the structure with minimum possibility of tunnelling. Because of the lower number of hydrogen atoms in the molecule (three hydrogen atoms per four anions) it is also necessary to consider the presence of the selenite anions. The corresponding vibrations ν_{as} and ν_s $SeO(SeO_3^{2-})$ at 723 and 810 cm^{-1}, respectively, were found in the IR spectrum. In agreement with the structure studies [19,20], the character of the IR spectrum for $KH_3(SeO_3)_2$ corresponded to the presence of two protons in ordered positions and one proton with a high tunnelling probability.

Shuvalov [242] described the crystal structure of the compound $(NH_4)H_3(SeO_3)_2$ on the basis of an X-ray structure study. This structure was refined by Tellgren [243] using neutron diffraction. Chomnilpan [244] carried out an X-ray structural analysis of the diselenite, $(NH_4)_2Se_2O_5$. Cesium gallium selenite hydrate, $CsGa_2H(SeO_3)_4{\cdot}2H_2O$,is monoclinic [245] with space group $12/b$ with $a = 14.15\ 8(2)$ Å, $b = 12.507(5)$ Å, $c = 7.736(1)$ Å and $\gamma = 102.59(2)^\circ$, $Z = 4$. The Ga atoms are octahedrally coordinated with Ga=O lengths 1.920 to 2.010 Å.

$Au_2(SeO_3)_2O$ was prepared [246] from gold and excess selenic acid in a sealed tube at 533 K. The crystal structure (*Pba*2, $a = 6.59.2(2)$ Å, $b = 11.837(3)$ Å, $c = 3.998(1)$ Å, $Z = 2$, $R = 0.087$) was determined. Gold atoms are bridged by oxide ions (lying on the two-fold axes) and selenite ions. The extended structure consists of polymeric layers parallel to the XY-plane. The light atom positions are inaccurate because of the presence of the heavy atom in a polar space group.

5. Studies on miscellaneous hydrogen selenites

5.1. Miscellaneous studies on some normal and transition metal hydrogen selenites

Boldt [247] determined crystal structure of 12 hitherto unknown acid selenites of divalent metals. These compounds have O–H···O distances of the hydroxyl groups between 2.81 and 2.56 Å. The IR spectra [247] exhibit double or triple bands in the V(OH) stretching mode region. Thus, these selenites form a system of normal, strong and very strong hydrogen bonds. They seem suitable for studying the transition between normal and very strong H-bonds. Therefore, and as a contribution to the nature of the ABC bands, Unterderweide et al. [30] presented the relations between the structural and spectroscopic data of quite a few hitherto unknown and known acid selenites.

Fig. 18 depicts the IR spectra of four selected hydrogen selenites as a function of the strength of

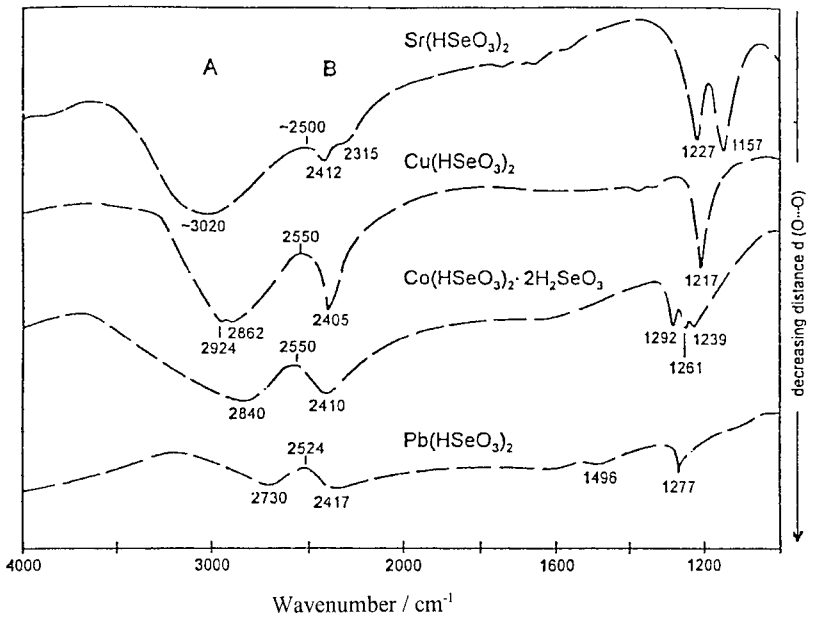

Fig. 18. IR spectra of four selected hydrogen selenites as a function of H-bond strength. Adapted from [30].

the H-bonds. The corresponding O–H···O bond distances d(O···O) range from 2.80 Å ($Sr(HSeO_3)_2$) to 2.57 Å ($Pb(HSeO_3)_2$). In the ν(OH) stretching mode region (3500–2000 cm^{-1}) there are always two distinct bands A and B, Fig. 18. This finding is independent of the number and type of the O–H···O bonds in the corresponding crystal structures. With decreasing O–H···O distance, the A band is strongly shifted to lower wave numbers; whereas the B band and the AB band 'gap' frequencies are nearly constant. At the same time the intensities of both bands, A and B, decrease with decreasing O–H···O bond distance. In the region of the δ(OH) in-plane bending modes (1300–1100 cm^{-1}), the band shapes, the frequencies and the number of the bands depend on both the O–H···O bond distances and the number of different H-bonds in the crystal structure. With decreasing O–H···O bond distance, the δ(OH) frequencies seem to increase and the intensities decrease. The IR spectra indicate [30] that the AB band doublets are produced by Fermi resonance of the ν(OH) stretching modes with the over tones of the bending vibrations 2δ(OH). The spectra show that the coupling increases with increasing H-bond strength. Because of the weak H-bonds [d(O···O) = 2.75 and 2.80 Å] in Sr $(HSeO_3)_2$, the overtone frequencies 2δ(OH) of the in-plane bending modes are relatively far from the stretching mode frequencies ν(OH). As a consequence, the Fermi resonance is also weak and the frequencies of the split B band almost correspond to the overtone frequencies 2δ(OH). In $Pb(HSeO_3)_2$, which exhibits strong H-bonds [d(O···O) = 2.57 Å], the ν(OH) and δ(OH) bands are shifted to lower and higher frequencies, respectively. Accordingly, the Fermi resonance interactions are stronger and the two bands, A and B, become broader and the intensities decrease.

The relevant structural and IR spectroscopic data of the compounds, shown in Fig. 18, and of all the other, investigated, selenites are summarized [30]. The sensitivity of ν_{as} to d(O···O) is rather great [30] with a nearly linear dependence. A similar correlation has been found for acid phosphates, arsenates and sulphates [248], but for these compounds all the ν_{as} are shifted to higher wave numbers by about 80 cm^{-1}, thus indicating that oxygen atoms in acid selenites are stronger proton acceptors than in the other named acid salts. Unterderweide et al. [31] in their excellent review on acid selenites have shown and interpreted many correlations of d(O···O) and spectroscopic data.

Engelen et al. [155] reported and discussed the crystal structures, IR, Raman and thermoanalytical

investigations of $M(HSeO_3)_2{\cdot}4H_2O$ (M = Mg, Co, Ni, Zn). The last three of these were new compounds. The crystal data of these isotypic compounds are reported [155]. The crystal structures consist of hexagonal packed $[M(HSeO_3)_2H_2O]_n$ chains of $[MO_4(H_2O)_2]$ octahedra linked by Se atoms. They contain trigonal pyramidal SeO_2OH ions with free hydroxyl groups and also 'free' molecules of water of crystallization. The hydroxyl groups build strong H-bonds (O–H···O distances: 2.65–2.68 Å). The IR spectra show AB doublet bands in the OH stretching mode region of the hydroxyl groups. The water molecules of crystallization are linked to planar $(H_2O)_4$ tetramers by H-bonds with unusually short O–H···O bond distances of 2.71–2.73 Å. DTA and TG measurements indicate that thermal decomposition results in the direct formation of the respective diselenite, MSe_2O_5.

Raman heating measurements under quasi static conditions show [155] the intermediate formation of the anhydrous hydrogen selenites.

The crystallographic data for the series of isostructural complexes $[Cu(HSeO_3)MCl_2(H_2O)_4]$ (M = Mn, Co, Ni, Cu, Zn) and $[Cu(HSeO_3)_2(H_2O)_2]$ and $[Cu(HSeO_3)_2(NO_3)_2]^{2-}{\cdot}2NH_4^+$ NH_4NO_3 [109] have been reported [109,110]. All these compounds have orthorhombic centrosymmetric space group *Pnma* [110] except $[Cu(HSeO_3)_2(H_2O)_2]$ which is monoclinic and has space group *P*21/*c* [109]. There are four formulae $[Cu(HSeO_3)_2\ MnCl_2(H_2O)_4]$ per unit cell. The structure consists of a three-dimensional net work [110], but it may be considered a layered one, the layers are almost the same as those encountered in $[Cu(HSeO_3)_2]$, $[Cu(HSeO_3)(H_2O)_2]$ and $[Cu(HSeO_3)_2(NO_3)_2]^{2-}{\cdot}2NH_4^+$. NH_4NO_3 [110]. The mass losses (Fig. 19) are compatible with the following reactions, which further support that the title compound has two water molecules of crystallization.

$$[Cu(HSeO_3)_2(H_2O)_2] \overset{(358-368\,K)}{\rightarrow} [Cu(HSeO_3)_2] + 2H_2O \quad (1)$$

$$[Cu(HSeO_3)_2] \overset{(473-503\,K)}{\rightarrow} CuSe_2O_5 + H_2O \quad (2)$$

$$CuSe_2O_5 \overset{(583-663\,K)}{\rightarrow} CuSeO_3 + SeO_2 \quad (3)$$

$$CuSeO_3 \overset{(748-813\,K)}{\rightarrow} \tfrac{1}{2}Cu_2OSeO_3 + \tfrac{1}{2}SeO_2 \quad (4)$$

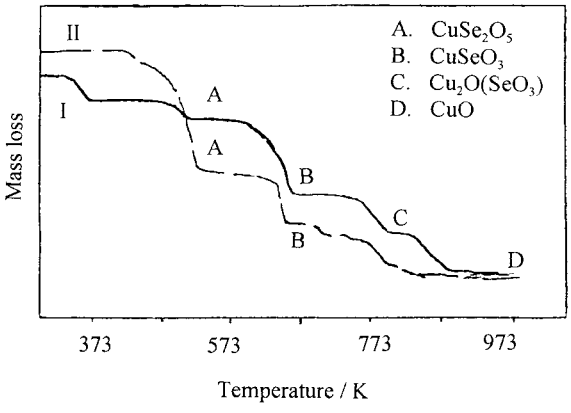

Fig. 19. Thermal curve of $[Cu(HSeO_3)_2(H_2O)_2\ ]$ (I) and $[Cu(HSeO_3)_2(NO_3)_2]^{2-}$ $2NH_4^+$, NH_4NO_3 (II). Adapted from [107].

$$\tfrac{1}{2}Cu_2OSeO_3 + \tfrac{1}{2}SeO_2 \overset{(823-933\,K)}{\rightarrow} CuO + \tfrac{1}{2}SeO_2 \quad (5)$$

All these anhydrous selenite phases have been prepared either by hydrothermal synthesis or by a solid state procedure [109]. Heating $[Cu(HSeO_3)_2(H_2O)_2]$ at varying temperatures offers a good technique to obtain the pure phase, except for Cu_2OSeO_3. It is noteworthy that $[Cu(HSeO_3)_2]$ is stable [109] between 358 and 473 K.

The first stage of decomposition of $[Cu(HSeO_3)_2(NO_3)_2]^{2-}{\cdot}2NH_4^+{\cdot}NH_4NO_3$ occurs [109] from 423 to 523 K, Fig. 19. This loss is in accordance with the formation of $CuSe_2O_5$. The second mass loss fits well with Eq. (3). The third loss is a multi-step process, and it is difficult to propose an interpretation, constant mass is not achieved until 848 K.

The powder XRD study in a heating cell (4 K h^{-1}) of $[Cu(HSeO_3)_2(H_2O)_2]$ shows [109] that this complex is decomposed around 358 K to yield well-crystallized $[Cu(HSO_3)_2]$. The latter phase is stable upto 473 K. The other selenites appearing in Fig. 19 are amorphous unless copper oxide crystallizes at 823 K. $[Cu(HSeO_3)_2(NO_3)_2]^{2-}2NH_4^+{\cdot}NH_4NO_3$, decomposes [109] around 408 K giving rise to amorphous compounds until CuO crystallizes.

5.2. *Miscellaneous studies on rare-earth hydrogen selenites*

According to the TG curves of Gd, Y, and Lu hydrogen selenites their decomposition mechanism

can be represented [249] as (R = rare-earth element)

$$RH(SeO_3)_2 \cdot 2.5H_2O \xrightarrow{1} RH(SeO_3)_2$$

$$\xrightarrow{2} \tfrac{1}{2}R_2(SeO_3)_3 \xrightarrow{3} \tfrac{1}{2}R_2O_2SeO_3 \xrightarrow{4} \tfrac{1}{2}R_2O_3$$

DTA measurements reveal the endothermic nature of all reactions. The calculated mass changes agree with the observed ones. In the first reaction the water molecules are released in two stages. The stability of the anhydrous hydrogen selenite phase extends to 300°C, increasing from gadolinium to lutetium Table 7. The second reaction stage comprises a simultaneous release of SeO_2 and H_2O and formation of rare earth selenite. The decomposition temperature of $RE_2(SeO_3)_3$ does not change much along the rare earth series. This is in agreement with an earlier investigation [36]. In contrast to earlier reports [250,251], the stability of the oxyselenite phase obtained decreases with decreasing ionic radius of the RE, Table 7. The lanthanum hydrogen selenite behaves exceptionally. Firstly, the composition and the structure of the starting compound differ from the others. Secondly, the mass change to oxyselenite does not correspond well to the calculated value. Thirdly, the diffraction diagram of the oxyselenite phase differs from that of Gd, Y and Lu compounds and the diagram shows similarities to that of $La_2O_2SO_4$. Finally, the luminescence spectrum of the lanthanum compounds was unresolved.

The formation and stability of the crystalline oxyselenite phase can be monitored [249] by measuring the luminescence spectra of the samples fired isothermally at various temperatures. The Eu^{3+} luminescence depends sensitively on the host compound. Moreover, the spectra fine-structure becomes unresolved for badly crystallized or multiphase materials. The optimum firing temperatures found with the aid of luminescence were 970 K for $(GdO)_2SeO_3$ and 920 K for $(LuO)_2SeO_3$ [249].

Table 7
DTG peak temperatures (K) for the decomposition reactions of $RH(SeO_3)_2 \cdot 2.5H_2O$. The reaction numbers correspond to those presented in the decomposition scheme, except the La compound

R	Reactions [248]			
	1	2	3	4
La	480	750	1065	1275
Gd	410	700	980	1200
Y	410	750	1000	1180
Lu	385	805	955	1105

Until recently there has been very little work, structural or otherwise, reported on phases containing rare-earth elements in combination with selenite anions [59]. The structures of $PrH_3(SeO_3)_2(Se_2O_5)$ [130], $CeSe_2O_6$ [252] and $NaLa(SeO_3)_2$ [253], $Nd(HSeO_3)(SeO_3)\cdot 2H_2O$ [131], $R_2Se_4O_{11}$, $R_4Se_7O_{20}$, $R_2Se_3O_9$ or R_2SeO_5 [136,254], and $Eu_2Se_5O_{13}$ [255] have recently been reported. These phases consist of the lanthanide atom in typical high coordination to oxygen, the coordination number depending on its ionic radius, 8 for Ce, r $Ce^{4+} = 1.28$ Å, 9 for Pr, r $Pr^{3+} = 1.32$ Å and 10 for La, r $La^{3+} = 1.40$ Å, linked into a three-dimensional structure via the sharing of faces and/or edges with other Ln–O (Ln = lanthanide) polyhedra, and vertices with the trigonal-pyramidal SeO_3 units.

The structure of $LaHSe_2O_6$ [59] is orthorhombic, Mr = 393.83 with space group $Pc2_1.b$, $Z = 8$, $V = 1149.24$ Å^3, $Dx = 4.55$ kg m^{-3}, $\mu = 199.7$ cm^{-1}. This new structure consists of layers of $LaO_{10}HSeO_3$ and SeO_3 polyhedra parallel to the *ac*-plane. The layers are interconnected by Se–OH···O–(Se, La) hydrogen bonds.

$NaY(SeO_3)_2$ is orthorhombic with $P2_{1cn}$ and $NaLa(SeO_3)_2$, monoclinic, $P21/n$. Structural data are reported [253]. Both structures contain discrete SeO_3 groups and pentacoordinate sodium. The yttrium atom in $NaY(SeO_3)_2$ is coordinated by seven oxygens in a distorted capped trigonal prism, while the lanthanum atom in $NaLa(SeO_3)_2$ adopts ten coordination based on a distorted bicapped square antiprism.

5.2.1. Structural studies on new praseodymium hydrogenselenite, $Pr_2(HSeO_3)_2(SeO_3)_2$

The crystal structure [132], solved by X-ray single crystal methods, is isostructural with $LaHSe_2O_6$ [59]. Although the Pr ionic radius is smaller than that of La, the Pr coordination number is ten. The simultaneous existence of double-edge and single-corner sharing selenite groups with praseodymium polyhedra, as well as the hydrogen bonding between the sheets present (H atoms localized), is emphasized. This compound has orthorhombic light green platelets with space group $Pbc2_1$, and $Z = 4$.

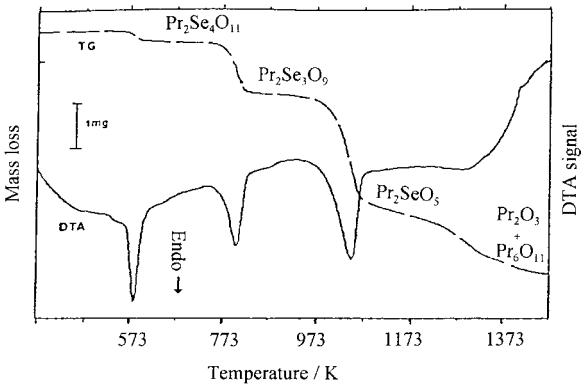

Fig. 20. Thermal behaviour of $Pr_2(HSeO_3)_2(SeO_3)_2$. Adapted from [132].

The first stage of the thermal decomposition (TG, DTA) of $Pr_2(HSeO_3)_2(SeO_3)_2$ starts [132] at 547 K and is complete at 623 K, Fig. 20. It corresponds [193] to the loss of one molecule of water, leading to an anhydrous praseodymium selenite, $Pr_2Se_4O_{11}$.

The second process, 643 to 828 K, is attributed to the further decomposition of this phase with the elimination of one molecule of SeO_2 giving rise to another anhydrous praseodymium selenite of composition $Pr_2Se_3O_9$, whose thermal behaviour has been described [254]. Similar behaviour is expected for the isostructural phases $Nd_2Se_4O_{11}$ and Nd_2 Se_3O_9, respectively, isolated in the thermal decomposition of $Nd(HSeO_3)(SeO_3)\cdot 2H_2O$ [131]. The DTA curve shows [132] three endothermic peaks, Fig. 20, in accordance with the three first mass losses, and one exothermic process due to the elimination of the last SeO_2 molecule, to yield Pr_2O_3, and its simultaneous oxidation to more stable praseodymium oxide, Pr_6O_{11}.

When the heating and cooling of these decomposition processes is carried out very slowly, the two first anhydrous praseodymium selenites, $Pr_2Se_4O_{11}$ and $Pr_2Se_3O_9$, can be isolated as tiny single crystals [132], while the last one, Pr_2 SeO_5, is always obtained as microcrystalline powder.

The IR spectrum of $Pr_2(HSeO_3)(SeO_3)_2$ permits the verification of the existence of SeO_3^{2-} and $HSeO_3$ groups. In fact, this spectrum exhibits [132] the classical vibrations between 440 and 840 cm^{-1}, attributed to the selenite anion, as well as another band at 1265 cm^{-1}, ascribed to $HSeO_3$ [106,123].

Magnetic measurements on $Pr_2(HSeO_3)_2(SeO_3)_2$ confirm [132] trivalent praseodymium. While the expected theoretical magnetic moment is 3.58 Bohr Magneton for one Pr(III), the mean experimental value is 3.48 Bohr Magneton, which confirms the 3+ oxidation state of the praseodymium and may involve a possible interaction between neighbouring cations [132]. The most exciting feature found in crystal structure of $Pr_2(HSeO_3)_2(SeO_3)_2$ is the simultaneous existence of tri-monodentate and bi-bidentate selenite groups, which bridge five metallic centres [132], giving rise to relatively small Pr–Pr distances. This fact opens up the possibility of finding interesting magnetic properties (antiferromagnetic coupling), so a more accurate study of the magnetic behaviour of this compound is now in progress [132].

5.2.2. *A general thermal decomposition scheme of rare-earth hydrogen selenites*

The anhydrous rare-earth selenites described upto now can be considered to be related, because they can be obtained by consecutive thermal decompositions of the hydrated or hydrogen selenites respectively [131,132,254]. In this way a general decomposition scheme is proposed [190], independently of the crystal structure of these compounds.

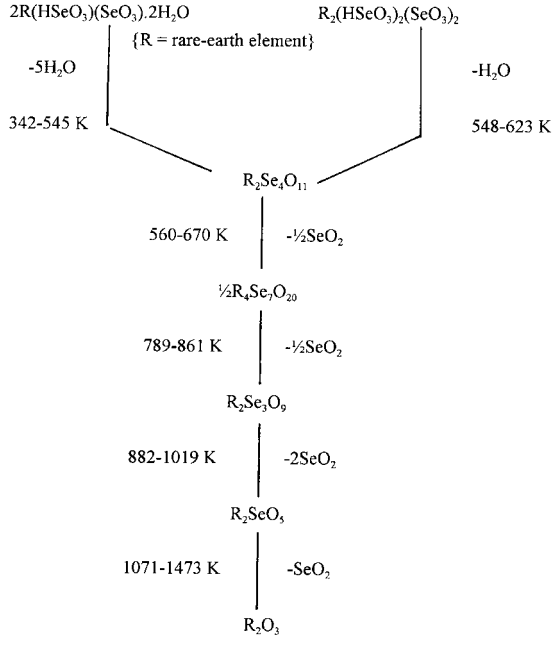

It is known that both hydrogenated selenites are constituted of infinite layers of R–O polyhedra,

HSeO_{ 3} and SeO_3^{2-} groups, which are held together by H-bonds. Thus, the total loss of H_2O leading to an anhydrous material must be due to the reaction of two hydrogen selenite groups giving rise to one diselenite group, $R_2(Se_2O_5)(SeO_3)_2$ being the correct formula of the corresponding selenite. This compound would exhibit a three-dimensional framework, built up by the connection of the starting layers of hydrogen selenite. Taking into account these facts, the decomposition processes of the anhydrous rare-earth selenites must be formulated as

$$R_2(Se_2O_5)(SeO_3)_2$$
$$\downarrow \; -\tfrac{1}{2}SeO_2$$
$$\tfrac{1}{2}R_4(Se_2O_5)(SeO_3)_5$$
$$\downarrow \; -\tfrac{1}{2}SeO_2$$
$$R_2(SeO_3)_3$$
$$\downarrow \; -2SeO_2$$
$$R_2O_2(SeO_3)$$
$$\downarrow \; -SeO_2$$
$$R_2O_3$$

6. Further scope

There is a rich structural chemistry of sodium lanthanide selenites [253], which is readily accessible using hydrothermal synthetic techniques. The stereochemically active lone pair on the selenium atom, in conjunction with high, often irregular, coordination around lanthanide atoms, may be an excellent combination in the search for novel asymmetric structures. Such material could have useful non-linear properties with potential applications in electro-optical devices.

$LaHSe_2O_6$ is the first layered anhydrous selenite to be discovered, complementing the layered $PrH_3(SeO_3)_2(Se_2O_5)$ [130] and layered hydrated selenite phases such as $CaSeO_3{\cdot}H_2O$ [217], and $LnHSe_2O_6{\cdot}2H_2O$, {Ln = Y, Pr to Yb (except Pm)}. The two-dimensional structure of $LaHSe_2O_6$, which is layered with respect to the polar crystallographic direction, combined with the acidic protons which must be present, leads to interesting possibilities for ion exchange and intercalation chemistry.

Studies have shown [165] that hydrothermal synthesis is an excellent method to produce new selenite materials containing metals from all parts of the periodic table. The conditions of the reactions (synthesis) are of vital importance in determining the final products, e.g., the aluminium coordination and the type of selenite ion produced, and variation of these conditions could lead to other new phases, e.g., a more alkaline reaction mixture may produce selenite compounds containing tetrahedral aluminium. Furthermore, there is, obviously, much scope for the preparation of gallium and iron analogues of the aluminium selenites.

The most exciting feature found in the crystal structure of $Pr_2(HSeO_3)_2(SeO_3)_2$ is the simultaneous existence of tri-monodentate and bi-bidentate selenite groups, which bridge five metallic centres giving rise to relatively small Pr–Pr distances. This fact opens up the possibility of finding interesting magnetic properties.

Acknowledgements

I am thankful to the Principal, R.E.C. Srinagar and the Coordinator R.E.C. Camp Jammu for enabling me, partially, to survey literature. My loving thanks to my son Er. Virendra for assisting me efficiently in the figure work. My immense thanks are to Prof. B.L. Khandelwal, FNAS, formerly Professor at IIT Delhi, presently Emeritus Scientist, CSIR, DMSRDE, Kanpur, India for introducing me to STDA, the only association of its kind, the world over. Because of this I am able to quote the latest work on selenium/selenites easily. For this my thanks are also due to the Chairman Prof. J.E. Oldfield and Mr. Yves Palmieri, Secretary STDA, for keeping me on their regular mailing list. I am highly grateful to all the Scientists and Researchers who readily sent reprints of their valuable work, to mention just a few, Dr J.C. Trombe, Centre for Materials and Structural studies, Electro Optical Laboratories CNRS, France, Dr. B. Engelen, Siegen University, Siegen, Germany, Dr. A.K.Chee-

tham USA/India; Dr. M. de Pedro, Institute for Materials, C.S.I.C, Serpano, Madrid, Spain; Dr. M. Wildner and Dr. G. Giester, Institute of Mineralogy and Crystallography, University of Wien, Austria and Prof. M. Ebert and Prof. Z. Mica, Department of Inorganic Chemistry, Charles University, Prague. My thanks go also to Prof M.E. Brown of Rhodes University, South Africa, for assistance in the preparation of this manuscript.

References

[1] V.P. Verma, Thermochim. Acta, 89 (1985) 363, and the references therein.
[2] P. Ray, A.N. Ghosh, J. Ind. Chem. Soc. 13 (1936) 494.
[3] H.L. Riley, J. Chem. Soc. (1928) 2985.
[4] G.V. Derbisher, Russ. J. Inorg. Chem. 5 (1960) 699.
[5] V.F. Toropova, Zh. Neorg. Khim. 2 (1957) 515.
[6] H.G. Geering, E.E. Cary, L.V.P. Jones, Wo Halaway, Soil Sci. Soc. Am. Proc. 32 (1961) 35.
[7] K. Sathianandan, L.D. McCory, J.L. Margrave, Spectrochim. Acta 20 (1964) 957.
[8] W.T.A. Harrison, L.L. Dussack, T. Vogt, A. Jacobson, J. Solid State Chem. 120 (1995) 112.
[9] J.T. Vaughey, W.T.A. Harrison, L.L. Dussack, A.J. Jacobson, Inorg. Chem. 33 (1994) 4370.
[10] W.T.A. Harrison, L.L. Dussack, A.J. Jacobson, Inorg. Chem. 33 (1994) 6043.
[11] R.E. Morris, A.K. Cheetham, Chem. Mater. 6 (1994) 67.
[12] Z. Micka, M. Ebert, Coll. Czech. Chem. Comm. 51 (1986) 1933.
[13] J. Loub, Z. Micka, J.P. Jana, M. Karel, K. Juergon, Coll. Czech. Chem. Comm. 57 (1992) 2309.
[14] Z. Micka, M. Ebert, P. Patacek, Coll. Czech. Chem. Comm. 51 (1986) 2741.
[15] S. Muspratt, J. Chem. Soc. 2 (1950) 59.
[16] J. Eyseltova, Z. Micka, M. Walzelova, Chem. Pap. 46(4) (1992) 218.
[17] A.K. Jokuziene, I.V. Yanitskii, Electroosazhdeniya Metal (Russ), 2 (1973) 34, cf. CA 81 (1974) 9076j.
[18] M. Ebert, D. Havelicek, Coll. Czech. Chem. Comm. 6 (1981) 1740.
[19] A. Simon, R. Paetzold, Z. Anorg. Allg. Chem. 301 (1959) 246.
[20] A. Simon, R. Paetzold, Z. Anorg. Allg. Chem. 303 (1960) 39.
[21] C. Rocchiccioli, Ann. Chem. 5 (1960) 1023.
[22] C. Rocchiccioli, Comput. Rend. 250 (1960) 2347.
[23] M. Ebert, D. Havlicek, Chem. Zvesti 34 (1980) 441.
[24] M. Ebert, D. Havlicek, Coll. Czech. Chem. Comm. 47 (1982) 1923.
[25] I.V. Yanitskii, S. Stasiene, Zh. Neorg. Khim. 30 (1985) 2149.
[26] T. Losoi, J. Valkonen, Finn-Chem. Lett. 1 (1984) 1.
[27] L.F. Nilson, Bull. Soc. Chim. Fr. 21 (1874) 253.
[28] Z.L. Leshchinskaya, N.M. Selivanova, Zh. Neorg. Khim. 11 (1966) 260.
[29] L. Neal, C.R. McCrosky, J. Am. Chem. Soc. 60 (1938) 911.
[30] K. Unterderweide, B. Engelen, K. Boldt, J. Mol. Str. 322(1–3) (1994) 233.
[31] R.E. Morris, W.T.A. Harrison, G.D. Stucky, A.K. Cheetham, J. Solid State Chem. 94 (1991) 227.
[32] R.E. Morris, W.T.A. Harrison, G.D. Stucky, A.K. Cheetham, J. Solid State Chem. 99 (1992) 200.
[33] R.E. Morris, W.T.A Harrison, G.D. Stucky, A.K. Cheetham, Acta Crystallogr., Sect. C., Cryst. Str. Comm. C48 (1992) 1365.
[34] G. Gospodinov, Thermochim. Acta 180 (1991) 169.
[35] V.P.Verma, to be published.
[36] G.S. Savichenko, I.V. Tananaev, A.N. Volodina, Izv. Akad. Nauk; Neorg. Mater. 4 (1968) 369.
[37] I.V. Tananaev, A.V. Volodina, N.K. Bolshakova and K.I. Petrov, Izv. Akad. Nauk; Ser, Neorg. Materialy 4 (1975) 1063.
[38] G. Meunier, C. Svensson, A. Cary, Acta Crystallogr. B32 (1976) 2664.
[39] J. Bonvoisin, J. Galy, J.C. Trombe, J. Solid State Chem. 107 (1993) 171.
[40] G. Meunier, M. Bertaud, Acta Crystallogr. B30 (1974) 2840.
[41] G. Meunier, M. Bertaud, J. Galy, Acta Crystallogr. B30 (174) 2834.
[42] J.C. Trombe, A. Gleizes, J. Galy, Crit. Rev. Acad. Sci. 297 (1983) 667.
[43] J.C. Trombe, A. Gleizes, J. Galy, J.P. Renard, Y. Journaux, M. Verdaguer, Naiv. J. Chim. 11 (1987) 321.
[44] M. Wildner, J. Solid State Chem. 103 (1993) 341.
[45] M. Wildner, J. Solid State Chem. 113 (1994) 252.
[46] G. Giester, M. Wildner, J. Solid State Chem. 91 (1991) 370.
[47] R.E. Morris, A.P. Wilkinson, A.K. Cheetham, Inorg. Chem. 31 (1992) 4774.
[48] H. Effenberger, J. Solid State Chem. 70 (1987) 303.
[49] G. Giester, J. Solid State Chem. 103 (1993) 451.
[50] A. Rabenau, Angew. Chem., Int. Ed. Engl. 24 (1985) 1026.
[51] M.E. Davis, R.F. Labo, Chem. Mater. 4 (1992) 756.
[52] Krishnan Gopal, J. Chem. Mater. 7 (1995) 1265.
[53] A.S. Znamenskaya, L.N. Komissarova, V.I. Spitsyn, Zh. Neorg. Khim. 17 (1972) 1828.
[54] A.S. Znamenskaya, L.N. Komissarova, Russ. J. Inorg. Chem. 18 (1973) 458.
[55] L.N. Komissarova, A.S. Znamenskaye, Russ. J. Inorg. Chem. 19 (1974) 159.
[56] O. Eraemetsa, T. Pakkanen, L. Ninistoe, Suomen Kemi 46 (1973) B 330.
[57] E. Giesbrecht, J. Giolito, Ann. Acad. Brasil. Cienc. 39 (1967) 233.
[58] A.S. Znamenskaya, L.N. Komissarova, V.M. Shatskii, Russ. J. Inorg. Chem. 22 (1977) 1150.
[59] R.E. Morris, W.T.A. Harrison, G.D. Stucky, A.K. Cheetham, Acta Crystallogr., Sect. C., Str. Comm. C48 (1992) 1182.

[60] G. Meunier, M. Bertaud, J. Galy, Acta Crystallogr. B30 (1974) 2834.
[61] J.C. Trombe, A. Gleizes, J. Galy, Crit. Rev. Acad. Sci., Ser. 2 (1983) 297.
[62] G. Huan, J.W. Johnson, A.J. Jacobson, D.P. Goshorn, Chem. Mater. 3 (1991) 539.
[63] J.T. Vaughey, W.T.A. Harrison, L.L. Dussack, A.J. Jacobson, Inorg. Chem. 33 (1994) 4370.
[64] K.S. Lee, Y.U. Kwon, H. Namgung, S.W. Kim, Inorg. Chem. 34 (1995) 4178.
[65] W.T.A. Harrison, J.T. Vaughey, A.J. Jacobson, J.W. Goshorn, J. Solid State Chem. 116 (1995) 77.
[66] Y.U. Kwon, K.S. Lee, Y.H. Kim, Inorg. Chem. 35 (1996) 1161.
[67] K.P. Singh Muktawat, R.K. Singhal, S.K. Dabral, J.P. Rawat, Acta Cienc Indica Chem. 17C (1991) 119.
[68] V.P. Verma, A. Khushu, to be published.
[69] W.T.A. Harrison, G.D. Stucky, A.K. Cheetham, Eur. J. Solid State Inorg. Chem. 30 (1993) 347.
[70] Z.F. Shakhova, S.A. Morosanova, Russ. J. Inorg. Chem. 14 (1969) 994.
[71] W.T.A. Harrison, L.L. Dussack, T. Vogt, A.J. Jacobson, J. Solid State Chem. 120 (1995) 112.
[72] M. Koskenlinna, J. Valkonen, Acta Chem. Scand. A31 (1977) 611.
[73] B.L. Khandelwal, S.P. Mallela, Zh. Neorg. Khim. 25 (1980) 3019.
[74] B.L. Khandelwal, S.P. Mallela, Transition Met. Chem. 5 (1980) 235.
[75] M. Wildner, K. Langer, Phys. Chem. Min. 21 (1994) 294.
[76] M. Wildner, Acta Crystallogr. C48 (1992) 595.
[77] G. Giester, F.J. Pertlik, Alloys and Compounds 210 (1994) 125.
[78] G. Giester, Z. Allg. Anorg. Chem. (1996) submitted.
[79] G. Giester, Acta Chem. Sci. 49 (1995) 824; and the citations therein.
[80] G.F. Pinaev, V.P. Valkova, Obshch Prikl. Khim. 3 (1970) 33.
[81] G.F. Pinaev, V.V. Peakovskii, V.P. Volkova, Russ. J. Inorg. Chem. 15 (1970) 1060.
[82] M. Wildner, G. Giester, Z. Krist. Suppl: Issue No. 9 (1995) 249.
[83] G. Giester, M. Wildner, to be published.
[84] G. Giester, to be published.
[85] G. Giester, Monatsh. Chem. 127 (1996) 347.
[86] G. Giester, Z. Krist. 207 (1993) 1.
[87] G. Giester, Monatsh. Chem. 125 (1994) 535.
[88] G. Giester, Monatsh. Chem. 124 (1993) 1107.
[89] M. Wildner, J. Solid State Chem. 120 (1995) 182.
[90] M. Wildner, Acta Crystallogr. C48 (1992) 410.
[91] M. Wildner, Miner. Petrol. 48 (1993) 215.
[92] M. Wildner, Acta Crystallogr. C50 (1994) 336.
[93] M. Koskenlinna, J. Valkonen, Acta Chem. Scand. A31 (1977) 638.
[94] M. Wildner, Monatsh. Chem. 122 (1991) 585.
[95] M. Wildner, Z. Krist. 185 (1988) 499.
[96] K. Kohn, K. Indoue, O. Horie, S. Akimoto, J. Solid State Chem. 18 (1976) 27.
[97] O.J. Lieder, G. Gattow, Naturwissenschaften 54 (1967) 443.
[98] O.J. Lieder, G. Gattow, Naturwissenschaften 54 (1967) 318.
[99] M. Ebert, Z. Micka, I. Pekova, Coll. Czech. Chem. Commn. 47 (1982) 2069.
[100] A.V. P McManus, W.T.A. Harrison, A.K. Cheetham, J. Solid State Chem. 92 (1991) 253.
[101] W.T.A. Harrison, A.V.P. McManus, A.K. Cheetham, Acta Crystallogr. C48 (1992) 412.
[102] V.F. Toropova, Zh. Neorg. Khim. 1 (1956) 243.
[103] H. Effenberger, Z. Krist. 173 (1985) 267.
[104] H. Effenberger, Z. Krist. 175 (1986) 61.
[105] H. Effenberger, F. Pertlik, Monatsh. Chem. 117 (1986) 896.
[106] Z. Micka, M. Cermak, D. Niznansky, Coll. Czech. Chem. Comm. 55 (1990) 2441.
[107] L. Hiltunen, M. Leskela, L. Niinisto, M. Tammenmaa, Acta Chem. Scand. 39 (1985) 809.
[108] V.G. Gattow, Acta Crystallogr. 11 (1958) 377.
[109] A.M. Lafront, J.C. Trombe, Inorg. Chim. Acta 234 (1995) 19.
[110] A.M. Lafront, J.C. Trombe, J. Bonvoisin, Inorg. Chim. Acta 238 (1995) 15.
[111] G. Gospodinov, Monatsh. Chem. 124 (1993) 115 (Ger).
[112] L. Ya Markovskii, Yu.I. Kodosov, V.A. Smirnova, Zh. Neorg. Khim. 12 (1967) 1466.
[113] L.Ya. Markovskii, Ya.P. Sapozhnikov, Russ. J. Inorg. Chem. 6 (1961) 816.
[114] V.P. Verma, A. Khushu, J. Thermal. Anal. 35 (1989) 87.
[115] M. Ebert, Z. Micka, M. Uchytilova, Coll. Czech. Chem. Commn. 49 (1984) 1653.
[116] Z. Micka, M. Uchytilova, M. Ebert, Chem. Zvesti. 38 (1984) 759.
[117] M. Ebert, Z. Micka, I. Pekova, Chem. Zvesti. 36 (1982) 169.
[118] V.P. Verma, A. Khushu, Proc. 31st Int. Congress of IUPAC 1987, Sofia, Bulgaria.
[119] L.Ya. Markovskii, Ya.P. Sapozhnikov, Russ. J. Inorg. Chem. 5 (1960) 1283.
[120] J.J. Berzelius, Acad. Handl. Stockholm, 39 (1818) 13.
[121] E. Giesbrecht, I. Giolito, Ann. Acad. Bras. Cienc. 34 (1962) 37.
[122] E. Giesbrecht, I. Giolito, Ann. Acad. Bras. Cienc. 39 (1967) 233.
[123] L. Niinisto, M. Leskela, in: K.A. Gschneider Jr., L. Eyring (Eds.), Handbook on the Physics and Chemistry of Rare Earths, pp. 91–320, Elsevier, Amsterdam, NY, 1987.
[124] E. Giesbrecht, G. Vicentini, L. Barbieri, Ann. Acad. Bras. Cienc. 40 (1968) 453.
[125] G.S. Savchenko, I.V. Tananaev, A.N. Volodina, Inorg. Mater. 4 (1968) 965.
[126] E. Immonen, M. Koskenlinna, L. Niinisto, T. Pakkanen, Finn. Chem. Lett. 67 (1976).
[127] J. Galy, J.J. Bonnet, S. Anderson, Acta Chem. Scand. Ser. A33 (1979) 383.
[128] A. Jerez, A. Castro, C. Pica, M.L. Veiga, Thermochim. Acta 54 (1982) 99.
[129] C. Pico, A. Castro, M.L. Veiga, E. Gultierrez-Puebla, M.A. Monge, C. Ruiz-Valero, J. Solid State Chem. 63 (1986) 172.

[130] M. Koskonlinna, J. Valkonen, Acta Chem. Scand. A31 (1977) 457.
[131] M. de Pedro, R. Enjalbert, A. Castro, J.C. Trombe, J. Galy, J. Solid State Chem. 108 (1994) 87.
[132] A. Castro, R. Enjalbert, M. de Pedro, J.C. Trombe, J. Solid State Chem. 112 (1994) 418.
[133] G. Giester, Montash. Chem. 120 (1989) 661.
[134] H. Effenberger, J. Solid State Chem. 70 (1987) 303.
[135] J. Durand, N. Loukilli, M. Rafiq, L. Cot, Acta Crystallogr. C44 (1988) 6.
[136] M. de Pedro, I. Rasines, A. Castro, J. Mater. Sci. Lett. 12 (1993) 1637.
[137] P.R. Claude, Ann. Chim. 5 (1960) 165.
[138] B.L. Khendelwal, V.P. Verma, J. Inorg. Nucl. Chem. 38 (1976) 763.
[139] V.P. Verma, 4th Ann. Conf. Ind. Council of Chemists, 1985, Gorakhpur, India.
[140] V.P. Verma, B.L. Khandelwal, Ind. J. Chem. 11 (1973) 602.
[141] Z.V. Roschhina, N.N. Selivanova, Tr. Mosk. Khim. Tekhnol. Inst. 62 (1969) 37.
[142] K. Itoh, Y. Hirata, H. Masumura, E. Nakamura, K. Deguchi, Solid State Commn. 86 (1993) 381.
[143] N.M. Selvinova, Z.V. Roschhina, Z. Prikl. Khim. 43 (1970) 975.
[144] N.M. Selvinova, Z.V. Roshina, Tr. Mosk. Khim. Tekhnol. Inst. 67 (1970) 8.
[145] T.V. Klushina, O.N. Evstafieva, N.M. Salivanova, Zh. Neorg. Khim. 20 (1975) 291.
[146] Z. Micka, Thesis Charles Univ., Prague 1982.
[147] W.C. Hamilton, J.A. Ibers, Hydrogen Bonding in Solids, W.A. Benjamin, New York, Amsterdam, 1968, p. 85.
[148] V. Lenher, E.J. Wochter, J. Am. Chem. Soc. 47 (1925) 1522.
[149] T.V. Klushina, O.N. Evstafeva, N.M. Selivanova, Y.M. Khozhainov, A.Ya. Monosova, Russ. J. Inorg. Chem. 20 (1975) 160.
[150] V.K. Magataev, V.F. Glushkov, L.A. Shuvalov, Ferroelectric Lett. Sect. 15 (1993) 97.
[151] T.V. Klushina, O.N. Evstafeva, N.M. Selivanova, V.V. Lapin, Yu.M. Khozhainov, G.E. Kalenchuk, Russ. J. Inorg. Chem. 19 (1974) 163.
[152] T.V. Klushina, Candidates Thesis, Mandeleev Moscow Institute of Chemical Engineering, 1970.
[153] Z. Micka, P. Pikal, M. Ebert, Chem. Papers 39 (1985) 617.
[154] C. Rocchiccioli, C. R. Acad. Sci. (Paris) 247 (1958) 1108.
[155] B. Engelen, K. Boldt, K. Unterderweide, U. Baeumer, Z. Anorg. Allg. Chem. 621 (1995) 331.
[156] W.G.R. DeCamargo, D.P. Svisero, Ann. Acad. Brasil. Cienc. 40 (1968) 207.
[157] L.Ya. Markovskii, Yu.P. Sapozhnikov, Zh. Struct. Khim. 1 (1960) 346.
[158] R.Ya. Melnikova, V.N. Makatun, V.V. Pechkovskii, A.K. Potapovich, V.Z. Drapkia, Russ. J. Inorg. Chem. 23 (1978) 382.
[159] V.N. Makatun, R.Y. Melnikova, T.I. Barannikova, Koord. Khim. 1 (1975) 920.
[160] B. Simmingskold, B.R. Johnson, Glass. Tekn. Tidskr. 9 (1954) 131.
[161] V.P. Verma, A. Khushu, to be published.
[162] I.V. Korneeva, A.V. Noroselova, Russ. J. Inorg. Chem. 4 (1959) 1011.
[163] G. Gospodinov, D. Barkov, Z. Phys. Chem. (Munich) 171 (1991) 241.
[164] Mellor's Modern Inorganic Chemistry, in: G.D. Parkes (Ed.), Longmans & Green, London, 1963, p. 794.
[165] R.E. Morris, W.T.A. Harrison, G.D. Stucky, A.K. Cheetham, J. Solid State Chem. 94 (1991) 227.
[166] L.N. Komissarova, Z.N. Prozoyovskaya, V.F. Chuvaev, N.M. Koshinova, Zh. Neorg. Khim. 16 (1971) 45.
[167] B.L. Khandelwal, S.P. Mallela, Thermochim. Acta 33 (1979) 355.
[168] B.L. Khandelwal, S.P. Mallela, Thermochim. Acta 37 (1980) 261.
[169] V.P. Garberg, A. Stahl, M. Worholm, J. Hogberg, Biochem. Pharmacol. 37 (1988) 3401.
[170] S.S. Bakeeva, R.A. Muldagalieva, E.A. Buketov, A.S. Paskhim, Tr. Khim. Met. Inst. Akad. Nauk Kaz. SSR 15 (1970) 88.
[171] N.M. Selivanova, A.I. Maier, Z.L. Leshchinskaya, I.I. Baskova, Khim. I. Khim. Tekhnol. 12 (1969) 1175.
[172] R.A. Muldagalieva, A.S. Pashinkin, E.A. Buketov, S.S. Bakeeva, Trudy Khim. Met. Inst. Akad. Nauk Kazakh. SSR 9 (1969) 11.
[173] V.V. Pechkovskii, V.N. Makatun, R.Ya. Melnikova, Russ. J. Inorg. Chem. 18 (1973) 1073.
[174] V.N. Makatun, Candidates Thesis, Minsk, 1970.
[175] M. Koskenlinna, L. Niinisto and J. Valkonen, Acta Chem. Scand. Ser. A 30 (1976) 836; .
[176] M. Koskenlinna, L. Niinisto and J. Valkonen, Cryst. Str. Commn. 5 (1976) 663.
[177] R. Miletich, A.O. Akad. Wiss. Math Naturwiss. K1 126 (1989) 77.
[178] V.N. Makatun, V.V. Pechkovskii, R.Ya. Melnikova, M.N. Ryer, Russ. J. Inorg. Chem. 19 (1974) 1851.
[179] V.G. Chukhlantsev, G.P. Tomashevskii, Zh. Anal. Khim. 12 (1957) 296.
[180] N.M. Selivanova, Z.L. Leshchinskaya, A.I. Maier, I.S. Streitsov, E.Y. Muzalev, Zh. Fiz. Khim. 37 (1963) 1563.
[181] S.S. Bakeva, E.A. Buketov, A.S. Pashinkin, Trudy Khim. Met. Inst. Akad. Nauk. Kazakh SSR 16 (1969) 9.
[182] N.M. Selivanova, Z.L. Leschinskaya, Zh. Neorg. Khim. 9 (1964) 259.
[183] V.F. Gladkova, Y.D. Kondrashov, Kristallografiya 9 (1964) 190.
[184] V.N. Makatun, V.V. Pachovskii, V.M. Goryaev, USSR Obshch Prikl. Khim. 2 (1970) 184.
[185] Gmelin Kraut, Handbuch der anorganischen chemie 7. Auft. Bd.5.Abt.2 (1914) 85.
[186] G.S. Savchenko, I.V. Tanaev, Izv. Akad. Nauk. Neorg. Mater. 44 (1968) 1097.
[187] Yu.B. Perkovskaya, Metody Poluch. Khim. Reactivov Prep. 16 (1967) 116 (Russ.).
[188] L.Y. Markovskii, R.A. Safina, Zh. Prikl. Khim. (Leningrad) 41 (1968) 2537.
[189] A.I. Maier, Y.L. Suponitskii, Izv. Vyssh. Ucheb, Zaved, Khim. Khim. Teckhnol. 14 (1971) 3.

[190] L.Y. Markovskii, R.A. Safina, Zh. Prikl. Khim. 41 (1968) 693.
[191] M. de Pedro, J.C. Trombe, A. Castro, J. Mater. Sci. Lett. 14 (1995) 994.
[192] C.M. Marcanofermin, Ph.D. Thesis, Madrid, 1986.
[193] A. Castro, R. Enjalbert, D. Lloyd, I. Rasines, J. Galy, J. Solid St. Chem. 85 (1990) 100.
[194] Donnary and Nowacki, Crystal data, in Diffraction file (ASTM) Card No.20-0276, 1968.
[195] V.V. Pechkovskii, V.N. Makatun, Russ. J. Inorg. Chem. 15 (1970) 1058.
[196] F.A. Cotton, R. Francis, J. Am. Chem. Soc. 82 (1970) 2985.
[197] J.D. Brown, M.Sc. Thesis, University of Newcastle-upon-Tyne, 1971.
[198] K. Nakamoto, J. Fujita, S. Tanaka, M. Kobayashi, J. Am. Chem. Soc. 79 (1957) 4904.
[199] W. Stuart, T.L. Whatley, J. Inorg. Nucl. Chem 31 (1969) 1639.
[200] M. Vidali, P.A. Vigate, G. Bandoli, D.A. Clemente, U. Casellato, Inorg. Chim. Acta 6 (1972) 671.
[201] B.L. Kanandelwal, V.P. Verma, Ind. J. Chem. 13 (1975) 967.
[202] R.D. Shannon, Acta Crystallogr. A32 (1976) 751.
[203] E.L. Muetterties, L. Guggenberger, J. Am. Chem. Soc. 96 (1974) 1748.
[204] H.D. Flack, Acta Crystallogr. A39 (1983) 876.
[205] W.T.A. Harrison, L.L. Dussack, A.J. Jacobson, Acta Crystallogr. C51 (1995) 2743.
[206] R.K. Rastsvetaeva, V.I. Andrianov, A.N. Volodnia, Dokl. Akad. Nauk. SSSR 291 (1986) 352.
[207] M. Kunz, I.D. Brown, J. Solid State Chem. 115 (1995) 395.
[208] J. Valkonen, M. Koskenlinna, Acta Chem. Scand. A32 (1978) 603.
[209] F.C. Hawthorne, Can. Min. 22 (1984) 475.
[210] H. Muilu, J. Valkonen, Acta Chem. Scand. A41 (1987) 183.
[211] G. Giester, Monatsh. Chem. 123 (1992) 957.
[212] G. Giester, Monatsh. Chem. 122 (1991) 617.
[213] G. Giester, Min. Pet. 48 (1993) 227.
[214] G. Giester, to be published.
[215] G.F. Pinaev, V.P. Volkova, Zh. Neorg. Khim. 21 (1976) 1341, V.P. Volkova, Author's Abstract of Candidate's Thesis, Perm, 1976.
[216] G.G. Pineev, R.A. Stukan, E.F. Makarov, Russ. J. Inorg. Chem. 22 (1977) 939.
[217] F.C. Hawthorn, L.A. Groat, T.S. Ercit, Acta Crystallogr. C43 (1987) 2042.
[218] M. Wildner, N. Jb. Miner. Mh. 1990 (1990) 353.
[219] R. Miletich, Thesis, Univ. Vienna, 1990.
[220] J. Zemann, Oster Miner. Ges. 136 (1991) 21.
[221] R.K. Rastsvetaeva, G.K. Petrova, V.I. Andrianov, Dokl. Akad. Nauk SSSR, 270 (1982) 882.
[222] G. Gospodinova, L. Sukova, K. Petrov, Zh. Neorg. Khim. 33 (1988) 1975.
[223] R. Weiss, Acta Crystallogr. 20 (1966) 533.
[224] V.P. Verma, Ph.D. Thesis, I.I.T Delhi, 1974.
[225] Yu.D. Kondrashev, Yu.Z. Nozik, Kristallografiya 24 (1979) 586.
[226] K. Nakamoto, Infrared Spectra of Inorganic and Coordination Compounds, Wiley/Interscience, London, 2nd edn., 1970.
[227] T.V. Klushina, N.M. Selivanova, V.V. Lapin, Yu.M. Khozhainov, C.E. Kalenchuk, Zh. Neorg. Khim. 19 (1974) 2917.
[228] T.V. Klushina, N.M. Selivanova, V.V. Lapin, A.A. Novikova, Zh. Neorg. Khim. 13 (1968) 2917.
[229] T.V. Klushina, N.M. Selivanova, V.V. Lapin, N.V. Lapin, N.V. Fedyainov, Zh. Fiz. Khim. 43 (1969) 1398.
[230] T.V. Klushina, N.M. Selivanova M.Kh. Karapetyants, V.V. Lapin, N.V. Fedyainov, Thermodynamic and Thermochemical Constants, Izd. Nauka, Moscow, 1970, p. 152.
[231] O.N. Evstafeva, T.V. Klushina, Zh. Neorg. Khim. 18 (1973) 1459.
[232] Z. Micka, M. Ebert, P. France, P. Ptacek, Chem. Papers 40 (1986) 309.
[233] C.A. Cody, C.A. Lewit, J. Solid State Chem. 26 (1978) 281.
[234] C.A. Cody, R.A. Khanna, Ind. J. Pure Appl. Phys. 15 (1978) 296.
[235] P.K. Acharya, R.S. Narayan, Spectrochim. Acta A 29 (1973) 925.
[236] C.A. Cody, R.K. Khanna, Ferroelectrics 9 (1975) 251.
[237] S. Chomnilpan, R. Liminga, Acta Crystallogr. B 35 (1979) 3011.
[238] K. Vedam, J. Ohaya, R. Pepinshi, Phys. Rev. 119 (1960) 1252.
[239] J.K. Mohana Rao, M.A. Viswamitea, Acta Crystallogr. B 27 (1971) 2692.
[240] R. Tellgron, R. Liminga, J. Solid State Chem. 4 (1972) 255.
[241] S. Chomnilpan, R. Liminga, R. Tellgren, Acta Crystallogr. B 35 (1979) 2692.
[242] L.A. Shuvalov, N.R. Ivonov, N.V. Gordeeva, L.F. Kirpikhoikova, Kristallografiya 14 (1969) 658.
[243] R. Tellgren, R. Liminga, Acta Crystallogr. B 30 (1974) 249.
[244] S. Chomnilpan, Acta Crystallogr. B 36 (1980) 675.
[245] R.K. Rastsvetaeva, G.K. Petrova, V.I. Andrianov, Dokl. Akad. Nauk SSSR, 270 (1983) 882.
[246] P.G. Jones, G.M. Sheldrick, E. Schwarzmann, A. Vielmader, Z. Naturforsch. 38b (1983) 10.
[247] K. Boldt, Thesis, Universitat Siegen, 1994.
[248] B.K. Choi, M.N. Lee, J.J. Kim, J. Raman Spectrosc. 20 (1989) 11.
[249] M. Leskala, J. Holsa, Thermochim. Acta 92 (1986) 489.
[250] M.A. Nabar, S.V. Paralkar, Thermochim. Acta 15 (1976) 390.
[251] M.A. Nabar, S.V. Paralkar, Thermochim. Acta 17 (1976) 239.
[252] C. Delage, A. Carpy, A.H. Naifi, M. Gourselle, Acta Crystallogr. C 42 (1986) 1285.
[253] R.E. Morris, J.A. Hriliac, A.K. Cheetham, Acta Crystallogr. C 46 (1990) 2013.
[254] A. Castro, M. de Pedro, I. Rasines, J. Thermal. Anal. 40 (1993) 1109.
[255] J.C. Trombe, Private Communication, 1996.